Chapter 7

Optical and Electronic Properties of Carbon Nitride

David Cameron
School of Electronic Engineering, Dublin City University, Dublin 9, Ireland

1. Introduction
2. Historical Development of Carbon Nitride
3. Production Methods for Carbon Nitride
3.1. Chemical Vapor Deposition Methods
3.2. Physical Vapor Deposition Methods
3.3. High Pressure Methods
3.4. Electrolytic Methods
4. Structural Properties of Carbon Nitride
4.1. Crystallography
4.2. Vibrational Spectroscopy
4.3. Electronic Spectroscopy
4.4. Observed Bonding Structures in Carbon Nitride
5. Electronic and Optical Properties
5.1. Internal Electronic and Optical Properties
5.2. "External" Electronic and Optical Properties
6. Conclusions
References

1. INTRODUCTION

Nitrogen-containing organic and polymeric carbon compounds have been known for many years, and even compounds containing only carbon and nitrogen, for example, so-called paracyanogen compounds that have a polymerized $(C{=}N)_n$ structure have been known and have been synthesized for some time [1]. Initial work on introducing nitrogen into carbon compounds

Supramolecular Photosensitive and Electroactive Materials, edited by H.S. Nalwa

ISBN 0-12-513904-7/$35.00

focused on the use of nitrogen for doping purposes such as into diamond crystals to make them semiconducting; N is now a well-known deep donor in diamond [2]. The first report of nitrogen-doping into amorphous carbon came in 1982 [3], and the initial intent was to modify the tribological properties, principally to reduce friction. However, interest in the formation of carbon–nitrogen compounds themselves, rather than as nitrogen-doped carbon, gained a major impetus following work in the mid-1980s by Cohen [4] and Sung [5], predicting the mechanical properties of a supposed crystalline form of carbon and nitrogen, carbon nitride, designated β-C_3N_4 by analogy with the structure of the β-form of silicon nitride β-Si_3N_4. If it existed, this material was postulated to be extremely hard, in fact similar in hardness to diamond with a very high bulk modulus. These predictions, not surprisingly, were followed by intense worldwide interest and many attempts to synthesize this material and also other predicted crystalline forms of carbon and nitrogen. Most of these attempts proved unsuccessful in producing crystalline material, but as time continued several groups have reported the deposition of thin films containing β-C_3N_4 and other crystalline structures by several different methods, with varying degrees of confidence, and the evidence for the existence of the material is now becoming much stronger. It is, however, not universally accepted; some workers consider the crystalline structures that have been found to be disordered polytypic diamond structures [6]. However, in addition to the crystalline material, there has been considerable reporting of the formation of amorphous films that have also been found to have unusual and interesting properties. It is clear then that there are two areas of research into the electronic properties of these materials that must be considered; amorphous carbon nitride, CN_x, and crystalline carbon nitride, β-C_3N_4 or some other structure. Furthermore, the amorphous material can be divided into those containing an appreciable amount of hydrogen that is normally produced by chemical vapor deposition (CVD) processes, possibly plasma or electron-assisted, in which there is a hydrogen content in the precursor gases or a hydrogen component in the gas mixture, and those containing no hydrogen, which are normally produced by physical vapor deposition (PVD) processes. This distinction, however, is not always as clear as it appears at first sight, because PVD deposited materials have also been shown to have appreciable hydrogen content in some cases as a result of contamination by hydrogen from residual gases.

It is the potential mechanical properties of the materials and their use for wear-resistant coatings that have provoked the most interest until now because of the aforementioned prediction of their superhard qualities. On the other hand, work on the electronic and optical properties is at a very early stage in which the basic behavior of the material is still being evaluated and a consensus on the results is still some way off and has been largely confined to

the amorphous materials. It is also clear that the various forms of amorphous CN_x or CN_x:H differ markedly in their properties. The studies that have looked in most detail at the electronic properties have been on materials with a rather low nitrogen and high hydrogen content. There have been very few studies that have measured the properties of films remotely approaching stoichiometry. In particular, the addition of hydrogen has been found to have a profound effect on the interatomic bonding within the compound and hence on the band structure and the optoelectronic properties. This account takes a broad view of the "electronic" in electronic properties.

As has been referred to in the preceding text, the doping of diamond crystals and thin films with nitrogen in an attempt to make an N-type material has been studied for many years now. The aim of that work is to produce semiconductors for use, for example, in high-temperature electronic devices. It is, however, not proposed to deal with the doped diamond material in this account, because the levels of nitrogen in the diamond are low and it can be considered as a substitutional doping effect rather than a distinct "carbon nitride" compound. This chapter concentrates on materials in which the nitrogen introduces some significant structural modification of the carbon material. In the following text, the term "carbon nitride" is applied generically as a shorthand term to the whole range of carbon materials with a significant nitrogen content and should not be assumed to imply a stoichiometric compound. If a particular form of carbon nitride is being considered, it will be made clear in the context whether it is crystalline or amorphous, stoichiometric, or otherwise.

The organization of this chapter is laid out as follows: Section 2 traces the history and development of carbon nitride and, in particular, the theoretical predictions of the atomic structure of the material. Section 3 deals with the methods that have been used to produce carbon nitride, which have, with few exceptions, been intended to deposit the material in thin film form on to a substrate. Section 4 outlines the current state of understanding of the structure of the material and, in particular, the interatomic bonding and its dependence on the electronic structure and the methods of its assessment Section 5 covers the theoretical and experimental work that has been carried out on the optoelectronic properties of carbon nitride, and Section 6 attempts to draw conclusions from the present state of knowledge and assess the prospects for further development.

2. HISTORICAL DEVELOPMENT OF CARBON NITRIDE

Before the current interest in carbon nitride materials, the only known solid compound of carbon and nitrogen was a polymer of overall formula $(CN)_n$

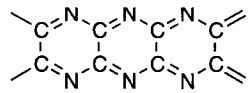

Figure 1 Atomic arrangement of the sp^2-bonded carbon–nitrogen compound that has the formula $(CN)_n$.

consisting of sixfold rings of alternate carbon and nitrogen in the form shown in Figure 1 with the carbon atoms having the sp^2 hybridization. This material can be prepared from the polymerization of cyanogen gas C_2N_2 but has the typical characteristics of a polymer in that it is soft and easily deformable. Thin films of paracyanogen material were synthesized directly from carbon and nitrogen in 1973 [7, 8] and also by ion-beam sputtering in 1979 [9]. In the initial publication of Cohen [4], which was later developed further [10, 11], it was suggested that carbon nitride could form a superhard compound. The initial argument was based on an empirical model for the bulk moduli of covalent solids. From previously known compounds and elements, two properties are required to achieve a large bulk modulus of elasticity — the prime requirement for a hard material. They are short bond lengths between adjacent atoms and a largely covalent nature of these bonds. From the properties of known hard compounds, Cohen and coworkers derived an empirical formula relating the bulk modulus B to N_c, the average coordination number of the atoms in the crystal, that is, the number of adjacent atoms to which they are bonded, λ the polarization factor of the bond, basically how "evenly" the electrons are shared between the two atoms, and D, the interatomic distance. They derived a formula

$$B = \frac{N_c}{4} \frac{(1972 - 20\lambda)}{D^{3.5}} \tag{1}$$

where B is in GPa and D is in Å.

This formula gave a good description of the bulk modulus of diamond and other tetrahedrally bonded materials. An empirical model based on different criteria was proposed by Sung [12]. This model known as the *PDC* model was calculated from the interatomic distance D, the average period number (in the periodic table) of the constituent elements P, and the degree of bond covalence C. He also derived a formula based on the characteristics of known hard materials given by

$$B = 12650 \times \frac{C^{0.318}}{P^{0.0806} D^{3.41}} \tag{2}$$

where B is in kbar (0.1 GPa) and D is in Å.

This formula was claimed to give a better prediction of the bulk properties because it included the period number of the elements of the compound, and

this, therefore, implicitly included a repulsive force between the atoms as a result of the larger number of core electrons in the higher period elements. Both formulas predict similar properties for carbon nitride crystals, depending on the exact crystal structure, which affects the bond length and bond angles. In both cases, the formula only strictly applies to purely tetrahedral compounds such as the diamond, zinc blende, or wurtzitic structures, whereas the suggested covalent carbon nitride compound C_3N_4 may not be stable in the zinc-blende structure but form a more complex covalent structure analogous to β-Si_3N_4 in which the C atoms are tetrahedrally bonded but the N atoms are trigonally bonded. Assuming that this crystal structure, shown in Figure 2, could be formed, Liu and Cohen [11] estimated the structural and electronic properties of the β-C_3N_4 arrangement using a first-principles pseudopotential total energy model based on the wurtzite structure. They determined the structural properties by calculating the total crystal energy as a function of volume. This value was determined to be 81 eV per cell or on average 5.8 eV per atom. This relatively large value suggested the possibility that the β-C_3N_4 structure may be stable or at least metastable. The C–N bond length calculated from this approach is 1.47 Å, which is intermediate between the sum of the C and N tetrahedral radii and the C tetrahedral and N trigonal radii. This value is in good agreement with the sum of the covalent radii of C and N when they are in the appropriate configuration [14, 15]. Fitting the total energy as a function of volume to the equations of state, as given by Murnaghan [16], gave a bulk modulus of 427 GPa, which is approximately 10% lower than the value calculated from the empirical formula. (The bulk modulus for diamond has been measured as ~440 GPa). A similar discrepancy between the values calculated for β-Si_3N_4 was also found. They also showed how the charge density in the

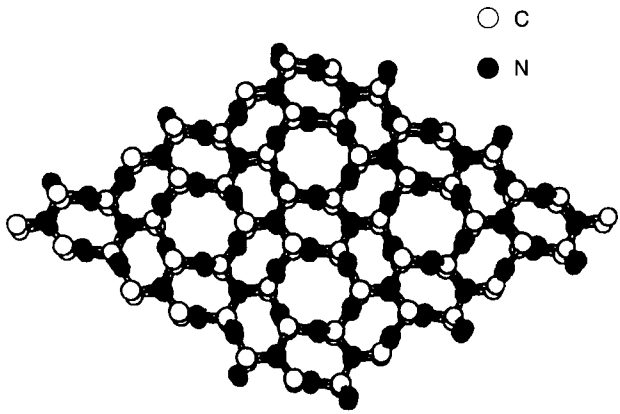

Figure 2 Crystal structure of β-C_3N_4 compound. After A. Y. Liu and R. M. Wentzcovitch, *Phys. Rev. B* 50, 10362 (1994).

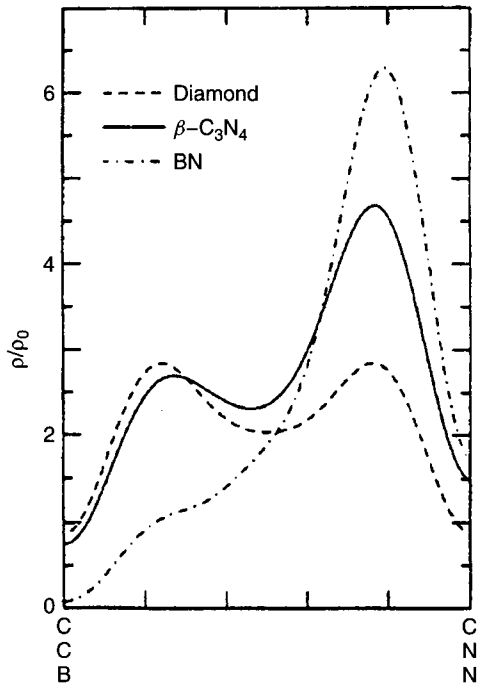

Figure 3 Charge density along the direction of the interatomic bond in diamond, cubic boron nitride (CBN), and β-C_3N_4. After A. Y. Liu and M. Cohen, *Science* 245, 84L (1989).

bond varies for three different bond types: the diamond C–C bond, the C–N bond in β-C_3N_4, and the B–N bond in cubic boron nitride. Figure 3 shows linear plots of the charge density along the direction of the bond between the atoms. It can be seen that the polarity of the bond lies between those of diamond and cubic boron nitride (cBN). The diamond C–C bond is symmetrical as would be expected from a totally covalent bond between like atoms with a double peak caused by the strong attraction potential of the C2p electrons; on the other hand, in boron nitride the charge is largely localized near the N atoms. The C–N bond in β-C_3N_4 lies between these two distributions and shows more of a covalent nature than cBN. The greater ionicity of the cBN bond when put into Eq. (1) indicates why β-C_3N_4 may have a higher bulk modulus than cBN.

It has also been postulated that other covalent phases of carbon and nitrogen might exist [12, 13, 17], for example, the α-form analogous to α-Si_3N_4, which is made up of an ABAB stacking sequence of layers of β-C_3N_4 (A) and its mirror image (B) , the zinc blende-type cubic form, a pseudocubic structure, and the rhombohedral graphite-like form. These structures are illustrated in

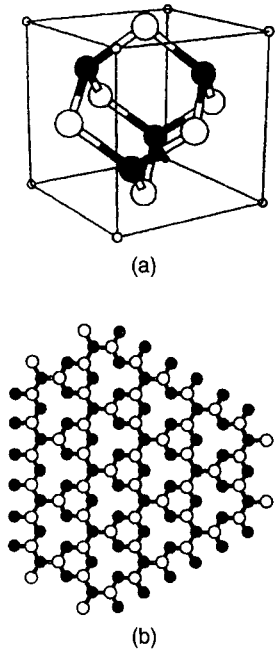

Figure 4 Alternative carbon nitride crystalline structures: (a) cubic (b) rhombohedral. After A. Y. Liu and R. M. Wentzcoritch, *Phys. Rev. B* 50, 10362 (1994).

Figure 4. The stability of these crystalline structures has been predicted from theoretical considerations [18]. It should be stated that the calculations of Guo and Goddard [17], based on a model that took account of the probability that the N atoms in C_3N_4 form nonplanar structures rather than the planar structure of the N atoms in β-Si_3N_4, predicted that the α-C_3N_4 structure would be thermodynamically the most stable and that its bulk modulus would be only 189 GPa, only 43% of that of diamond. However, they made the remarkable prediction that its Poisson ratio should be negative and this implies that stretching the structure in one direction should also cause it to expand in the orthogonal directions unlike any other known material. There have also been predictions of other possible carbon nitride structures and theoretical calculations of their likely properties. The density of states and band structures for fullerene-like [19] and nanotubular structures or other three-dimensional sp^2-bonded CN structures [20, 21] have been calculated. In fact, fullerene-like formations in carbon nitride films have been observed in transmission electron microscopy [22].

These calculations and predictions generated a large amount of interest in the production of carbon nitride materials and there have been many attempts

to produce the crystalline form by different methods that will be detailed in the following text. There have been relatively few reports of totally crystalline deposits being produced, although their numbers are now increasing significantly. However, most results reported till now have been of amorphous material or amorphous material containing a certain amount of a crystalline phase. The number of papers being produced on the deposition of carbon nitride films amounted to more than sixty published in the main scientific journals in the first half of 1999; however, there have still been few results published on the electronic or optical properties of the crystalline or even the amorphous material.

For industrial usage, the first U.S. patent referring specifically to carbon nitride was taken out in 1987 by the Victor Company of Japan [23]. This patent referred to the application of thin carbon nitride films as low-friction wear-resistant overcoatings for magnetic storage discs. This area remains the only commercial area of application up to the present. The first U.S. patent referring directly to the formation of the crystalline form of β-C_3N_4 was filed in 1992 [24].

3. PRODUCTION METHODS FOR CARBON NITRIDE

In considering the electronic and optical properties of carbon nitride, it is clear that the details of the structure have an enormous influence on the properties. Therefore, a general description of the various types of deposition process are given here as they have a major effect on the structure of the material. The production processes used for carbon nitride can be divided into four categories:

1. Chemical vapor deposition (CVD) processes in which the reactant materials are transported in the gas phase to the substrate where a chemical reaction takes place to form the carbon nitride, perhaps with the evolution of by-products.
2. Physical vapor deposition (PVD) processes in which the carbon and nitrogen are directly transported to the substrate in molecular, atomic, or ionic form where they combine directly to form the compound.
3. High-pressure and high-temperature methods that attempt to directly synthesize the carbon nitride under equilibrium conditions in the appropriate region of the carbon–nitrogen phase diagram.
4. Electrolytic methods.

Methods (1), (2), and (4) have been used to produce carbon nitride in thin film form, whereas method (3), which is similar in concept to the high-temperature and high-pressure process for the industrial production of individual diamonds,

is aimed at the production of discrete grains of the crystal. These processes are described in detail in the following text.

3.1. Chemical Vapor Deposition Methods

The CVD techniques for depositing carbon nitride involve activation of the reaction using as an energy source (a) thermal energy supplied, for example, by a hot filament (HFCVD) or furnace tube with the possible application of a DC bias between the filament and the substrate to create a plasma and accelerate the ions toward the substrate, (b) electromagnetic energy using, for example, radiofrequency or microwave excitation to create a plasma (PACVD), also with the possible addition of a substrate bias, or (c) a combination of these. In addition, the process of plasma-enhanced chemical transport (PECT), which is a chemical process involving the transformation of the film materials from the solid to the gas phase and their subsequent deposition from the gas to the solid phase at a different point, can also be considered as a CVD process.

3.1.1. Hot Filament CVD

Hot filament CVD is a method that has been widely applied to the deposition of diamond films [25]. It has been used as the basis for the deposition process of carbon nitride films by a number of workers, for instance, Chen and coworkers [26] and Leonhardt and coworkers [27]. A schematic diagram of the main features of such a system is shown in Figure 5. In this method, the precursor gases, which comprise a source of carbon such as methane CH_4

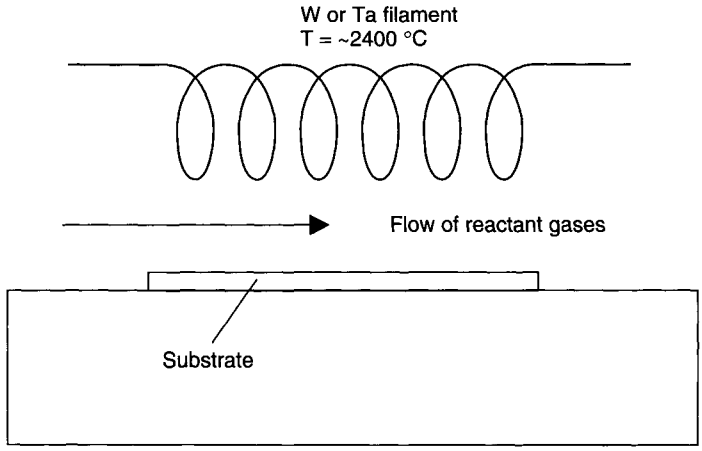

Figure 5 Schematic diagram of hot filament CVD deposition system.

or carbon monoxide CO and nitrogen gas, flow past a carburized tungsten or tantalum filament that is heated by the passage of an electric current to approximately 2400 °C. Additional diluent gases of argon and hydrogen may also be included [27]. The effect of the hot filament is to dissociate the gas molecules into atomic species, thereby enhancing their reactivity. The subsequent reaction then causes the deposition of a solid film on the adjacent substrate. It has been found that an additional source of energy such as a negative DC bias on the substrate to accelerate the ions toward it has been necessary to improve the film properties.

3.1.2. Plasma-Assisted CVD

The methods of producing carbon nitride films by PACVD have used radiofrequency (RF) or microwave frequency excitation as a source of energy for the chemical reaction. These methods have used either parallel plate [28, 29], inductively coupled [30], helical resonator [31] or electron cyclotron resonance (ECR) [32, 33] configurations. The schematic diagram of a typical RF-activated "parallel plate" capacitively coupled deposition system is shown in Figure 6; the chamber walls typically act as the grounded electrode. In the case of the inductively coupled system, a helical coil is used as the excitation source rather than a directly connected electrode. For the helicon system,

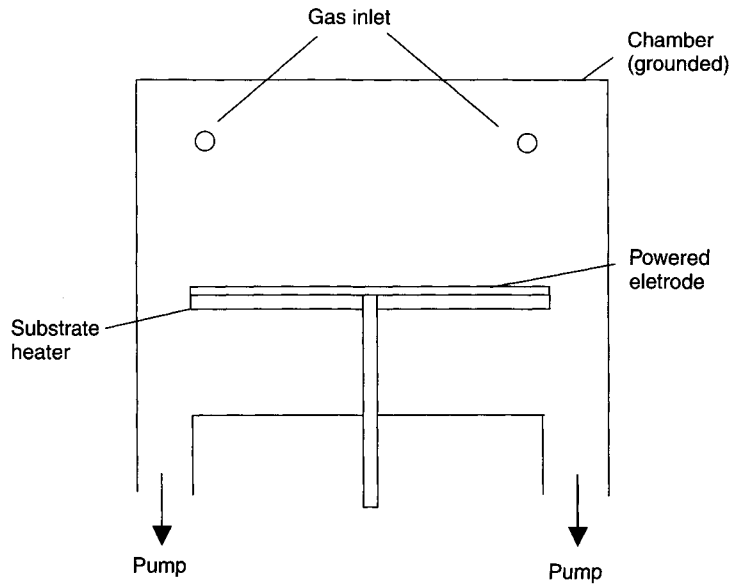

Figure 6 Schematic diagram of capacitively coupled PECVD deposition system.

the plasma is excited via radiofrequency power applied by a helical coil that along with the magnetic field in the plasma produces a resonant effect, providing efficient coupling of power into the plasma. Figure 7 shows a schematic diagram of a typical system. In the microwave ECR system, a longitudinal magnetic field is applied to bring about cyclotron resonance of the electrons in the plasma with the microwave energy, again resulting in efficient coupling of power and an intense plasma discharge. A typical system is shown schematically in Figure 8.

The gaseous precursors for these processes are generally a hydrocarbon gas as the source of carbon, typically methane CH_4 but also acetylene C_2H_2or ethylene C_2H_4. In some cases, other materials such as fullerenes, teracyanoethylene, or organometallic compounds containing 1,3,5-triazine groups, halogens, and alkyl groups [34] have been employed. The nitrogen-containing compounds mentioned earlier have a certain amount of carbon and nitrogen

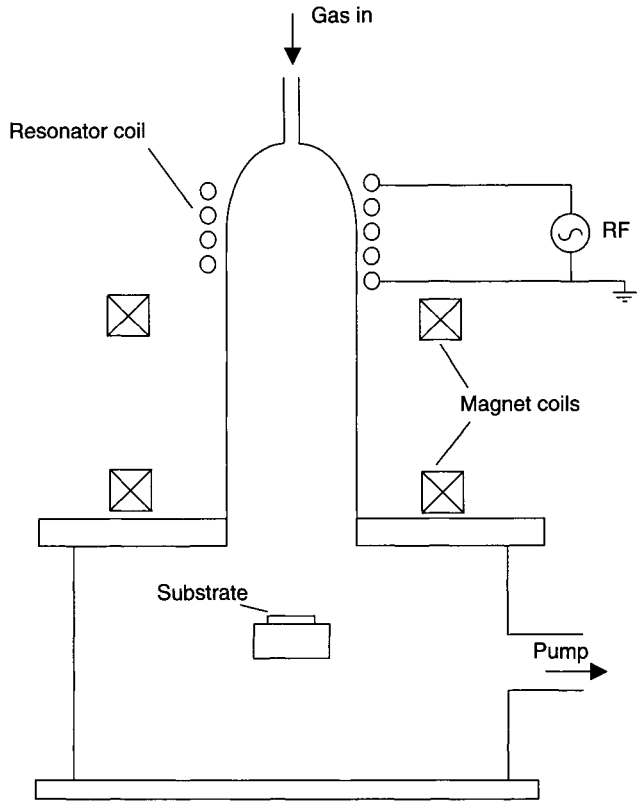

Figure 7 Schematic diagram of a helicon PECVD deposition system.

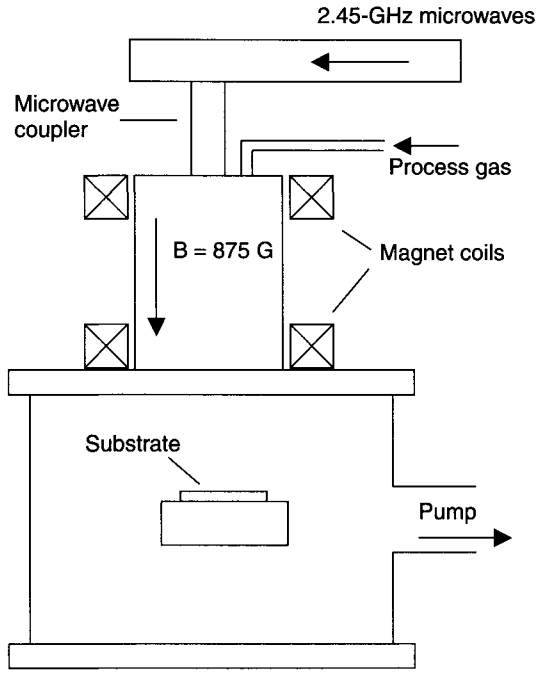

Figure 8 Schematic diagram of a microwave ECR PECVD deposition system.

bonded together in the same configuration as is desired in the deposited film, the aim being to maximize the C–N bonding in the film. The source of nitrogen is generally either nitrogen gas or ammonia NH_3, although an additional source of nitrogen is not necessarily required in the case of precursors that already include carbon and nitrogen such as the azine compounds. The main compositional feature of the films produced by these systems is that they generally contain a large proportion of hydrogen in their structure coming from the precursor chemicals, as is discussed later. Substrate biases ranging from 0 to 600 V have been applied in an attempt to affect the structure of the films thus formed. The substrate may be unheated (except for the energy input caused by plasma bombardment) or it may have an additional source of heat.

3.1.3. Plasma-Enhanced Chemical Transport

This process is a variant of the PACVD process whereby the carbon and nitrogen precursors are not all supplied externally but are generated in situ and transported to the substrate through the gas phase. For example, in the processes described by Vepřek [35] and Popov [36], nitrogen gas supplied externally is decomposed to atomic nitrogen in a RF plasma using inductive

or capacitive coupling. The atomic nitrogen then reacts with a solid graphite electrode to form a $(CN)_n$ precursor vapor, a bulk graphite insert within the reaction chamber in the process described by Veprek and a carbon mesh obtained by the combustion of cellulose fibres in the process described by Popov. The method of Matsumoto [37] is rather different. In this process, a thermal plasma torch is ignited by RF induction in near-atmospheric pressure nitrogen into which graphite powder is mixed by suspending it in an argon carrier gas, and a plasma-enhanced chemical transport process using a hollow cathode discharge in a graphite target has been used by Muhl and coworkers [38] and has produced crystalline material.

The enthalpy of formation of the various species in the carbon–nitrogen system is illustrated in Figure 9. The formation of CN radicals from carbon and molecular nitrogen is strongly endothermic, whereas their formation from atomic nitrogen is slightly exothermic [9, 35]. Thus the reaction

$$C(s) + N(g) \rightarrow CN(g)$$

occurs. These CN radicals are then transported to the substrate where by in the presence of excess atomic nitrogen, they can form a carbon nitride solid. It is possible that the absence of excess nitrogen atoms at the substrate leads to the formation of the paracyanogen $(CN)_x$ polymeric material. Figure 10 shows the apparatus used by Vepřek and coworkers in their work. They also predicted that a high deposition temperature would be necessary to obtain stoichiometric carbon nitride, first to avoid the formation of any paracyanogen content in the films because it would sublime above 800 °C and second by

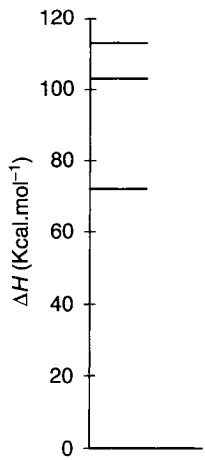

Figure 9 Enthalpy of formation of various species in the carbon-nitrogen system. After S. Vepřek, J. Weidmann, and F. Glatz, *J. Vac. Sci. Technol., A* 13, 2914 (1995).

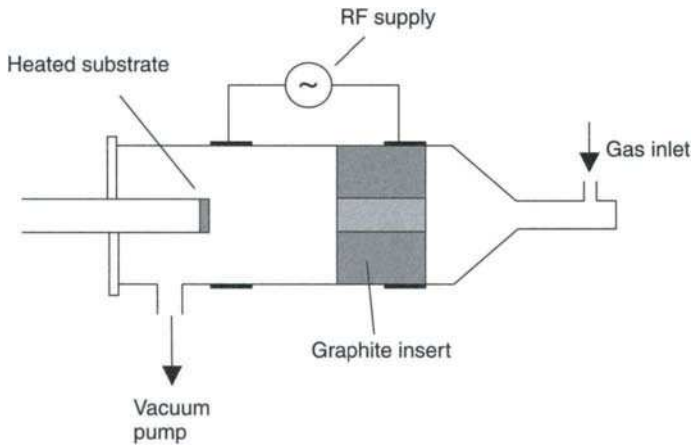

Figure 10 Diagram of PECT deposition system. After S. Vepřek, J. Weidmann, and F. Glatz, *J. Vac. Sci. Technol., A* 13, 2914 (1995).

analogy with silicon nitride in which the β-Si_3N_4 phase forms only above 1350 °C. As mentioned previously, in Popov's method, a carbon mesh was used as a source of carbon atoms to maximize the surface area of the carbon exposed to the atomic nitrogen and increase the reaction rate. By measuring the gas composition during deposition by a quadropole mass spectrometer, the presence of CN radicals in the reaction chamber was confirmed but no evidence that polymerization of these into $(CN)_2$ or higher species occurred was found.

3.2. Physical Vapor Deposition Methods

This category covers a very wide range of deposition methods in which the material is transported to the substrate in the form of carbon atoms or ions and nitrogen molecules, atoms, or ions. In this chapter, the author has not attempted to give an exhaustive review of all the variations in deposition processes but has described the main features of the most commonly used techniques. Because in these cases only the elements carbon and nitrogen are normally involved, the problem of incorporation of impurities such as hydrogen becomes less of an issue, but even here there is scope for contamination of the films by residual gases in the deposition system, in particular, water from the adsorbed layer that always forms when a surface is exposed to the atmosphere. The main techniques used are as follows:

1. Sputtering of a graphite target: This technique may be diode sputtering or one of the variations of magnetron sputtering, either using DC or

RF power to the target or by using a direct ion beam as the agent of removal of target material. The nitrogen is then incorporated by using a nitrogen atmosphere in the system that reacts on the substrate surface with the deposited carbon.

2. Laser ablation: In this technique, carbon is removed from the target by the thermal energy deposited in the target surface by a powerful laser beam and the plume of vaporized material then falls on the substrate. A nitrogenous atmosphere or a nitrogen ion beam impinging directly on the substrate produces the nitride compound.
3. Vacuum arc evaporation: In this technique, the carbon is evaporated from the graphite target by an arc discharge producing a flux of highly ionized carbon. Again a source of nitrogen such as an ion beam is used to form the nitride.
4. Evaporation of carbon atoms or clusters: The carbon may be ionized; it then falls onto the substrate where it reacts with the nitrogen atmosphere or with a flux of nitrogen ions from an ion gun.
5. Direct deposition from ion beams of carbon and nitrogen.
6. Direct implantation of nitrogen ions into a carbon substrate.

Many systems contain hybrids of these categories, for example, laser ablation and ion bombardment of the substrate. In these PVD methods, hydrogen is not an intentional constituent of the films; however, unintentional incorporation of hydrogen has been observed because of the presence of water vapor in the residual atmosphere during the deposition process, particularly at higher pressures, and this has been found to affect the nitrogen content in some cases [39].

3.2.1. Sputtering

Most of the films deposited by sputtering processes have used conventional DC planar magnetron sputtering of graphite in an atmosphere of nitrogen or an argon–nitrogen mixture. In this process, most of the carbon species are neutral carbon atoms that react on the substrate with nitrogen ions and neutrals to form a carbon nitride compound with a greater or lesser nitrogen content. There are numerous reports of this type of system [40–43] and the group of Sundgren at Linköping is notable [44]. RF-powered magnetron sputtering has also been used by several groups [45–47]. A nonconventional Penning-type-opposed target magnetron system has been used by Chowdhury and coworkers [48], and this system is claimed to have a higher ionization level than the normal magnetron configuration. A diagram of this type of configuration is shown in Figure 11. For magnetron sputtering, the pressure during deposition is typically in the region 0.1 to 1 Pa. Typically, RF bias is applied to the substrates, allowing the energy of the gaseous ions bombarding them to be independently

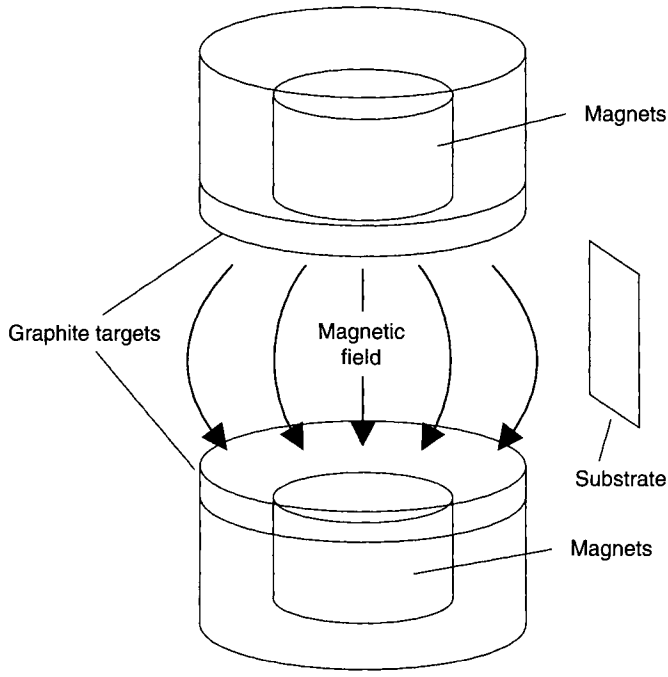

Figure 11 Schematic diagram of Penning-type-opposed target magnetron.

controlled. The substrates may also have heat applied during deposition, other than the energy that impinges as a result of depositing or bombarding species. Sputtering of the target material using ion beams instead of ions derived from a plasma has been used with graphite targets [49–51] and also for deposition from the biomolecular materials azaadenine $C_4N_6H_4$and adenine $C_5N_5H_5$ at lower pressure, approximately $2–4 \times 10^{-2}$ Pa [52, 53]. The advantage of these biomolecular target materials is that they already contain carbon and nitrogen in a ring structure that might be expected to facilitate the formation of crystalline carbon nitride. The molecular structure of these materials is shown in Figure 12.

3.2.2. Laser Ablation

This technique has been widely used for deposition of carbon nitride [54–57]. Figure 13 shows a typical arrangement for a deposition system. In most cases, either a Nd:YAG or a KrF excimer laser is used in the pulsed mode, the laser wavelengths ranging from 213 to 532 nm (Nd:YAG) and 248 nm (KrF). The beam is focused on a graphite target and the resulting

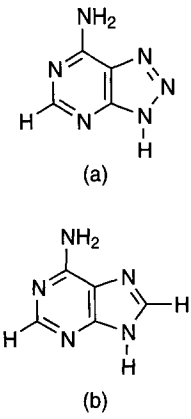

Figure 12 Molecular structure of the biomolecular materials (a) azaadenine and (b) adenine used as target material.

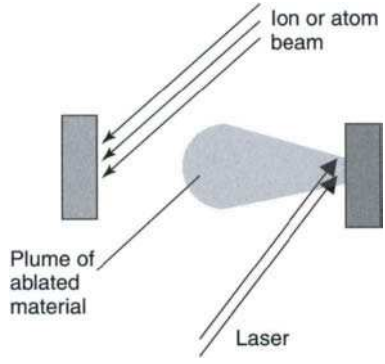

Figure 13 Typical arrangement of a laser ablation deposition system.

plume of carbon atoms is allowed to impinge on the substrate (which is also normally heated) in a nitrogen environment. This may be simply nitrogen or ammonia gas, but in many cases the substrate is irradiated by a nitrogen ion or atomic nitrogen beam to increase the likelihood of a nitrogen–carbon reaction. The pressure in the reaction chamber is in the range of 10^{-3}–100 Pa, depending on whether a particle beam is used.

3.2.3. Vacuum ARC Evaporation

Carbon nitride films have been deposited by a number of vacuum arc evaporation techniques, for example, anodic arcs [58] and various cathodic

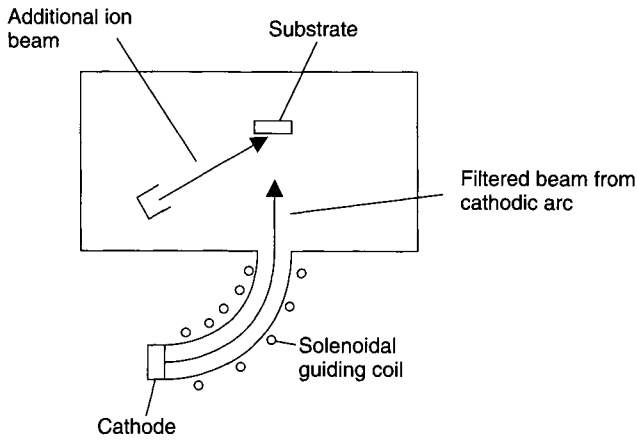

Figure 14 Schematic diagram of a filtered cathodic arc (FCA) deposition system.

arc methods. The cathodic arc evaporation method involves striking an arc between a negatively biased graphite target and an electrode. This method produces a highly ionized flux of carbon that can then deposit on to a substrate in the presence of nitrogen ions [59, 60]. The major problem with this technique is that the evaporated flux contains a large number of droplets of the cathode material that give rise to inclusions in the deposited film. To overcome this problem, the cathode cannot be allowed a line-of-sight view of the substrate, and this can be avoided either by shielding the substrate from direct view of the cathode [61] or by using the magnetic field from a curved solenoid to guide the ions from the cathode along a curved path such that the macro clusters of atoms, which are heavier than the individual ions, are not able to follow the lines of magnetic field and are therefore filtered out. This technique is known as the *filtered cathodic arc* (FCA) [62, 63]. The schematic outline of a typical system is shown in Figure 14. Other variations of the arc-deposition method involve directing a beam of nitrogen ions through an arc between graphite electrodes to obtain a mixed beam of nitrogen and carbon that then impinges on a substrate. Such a system has been described in a U.S. patent [64]. A different type of process using pulsed high-energy electron or ion bombardment of layers alternately of carbon or liquid nitrogen in a technique that has also been used for diamond synthesis [65] has been shown to produce carbon nitride films.

3.2.4. Carbon Evaporation

In this process, the carbon flux is obtained by evaporation of graphite, typically by an electron beam. To incorporate nitrogen into the film, a

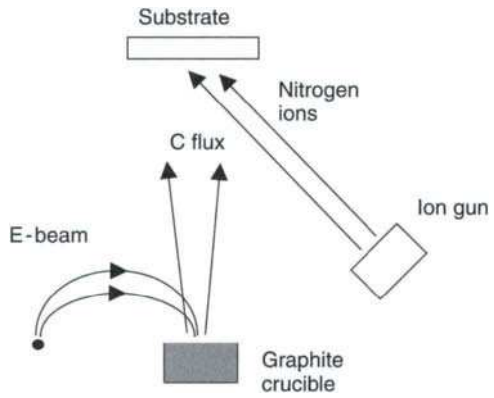

Figure 15 Schematic diagram of evaporated carbon deposition system.

nitrogen ion beam also irradiates the substrate surface [66, 67] as illustrated in Figure 15. An interesting variation of this technique has been described by Xie and coworkers [68]. In this system, the source of carbon is low-density polyethylene evaporated from a Knudsen cell. The flux of carbonaceous material that is formed of clusters rather than single atoms then passes through a plasma zone in which it is ionized to a high level. It then impinges on the substrate in the presence of nitrogen, which is also partly ionized by the plasma, to form the carbon nitride layer. This arrangement is shown in Figure 16.

3.2.5. Ion Beam Deposition

The method of direct deposition from ion beams has an advantage in terms of the control that can be exercised over the energy and the flux of the species arriving at the substrate compared with other methods in which control over these parameters can be indirect and interdependent. Early work by Mansour and Ugolini [69] used a mixture of methane and argon in one ion-beam source with 400 eV energy, whereas later work used hydrogen-free beams of mass-selected C^+ ions and N_2^+ or N^+ ions with energies in the range 5–350 eV [70]. Tsoubouchi and coworkers [71] used mass-separated beams of isotopically pure $^{12}C^{14}N^-$ ions in the range 50–400 eV produced from a plasma-sputtering negative ion source.

3.2.6. Ion Implantation into Carbon Films

There has been a limited amount of work on this method of formation of carbon nitrides. The process employs the implantation of low-energy N^+ [72,

73] or N_2^+ [74] ions into targets of tetrahedral amorphous carbon, graphite, or diamond. The work has been restricted to fundamental studies of the bonding in very thin surface layers because the energy of the bombarding ions has only been up to 20 KeV, allowing a penetration of N atoms up to a maximum of approximately 40 nm.

Among all the PVD methods described, the great majority of work has been carried out using reactive DC magnetron–sputtered films and the main reason for this is the simple deposition process and the relative availability of deposition equipment. There tend to be significant differences between the properties of the different PVD deposited films, particularly as regards the

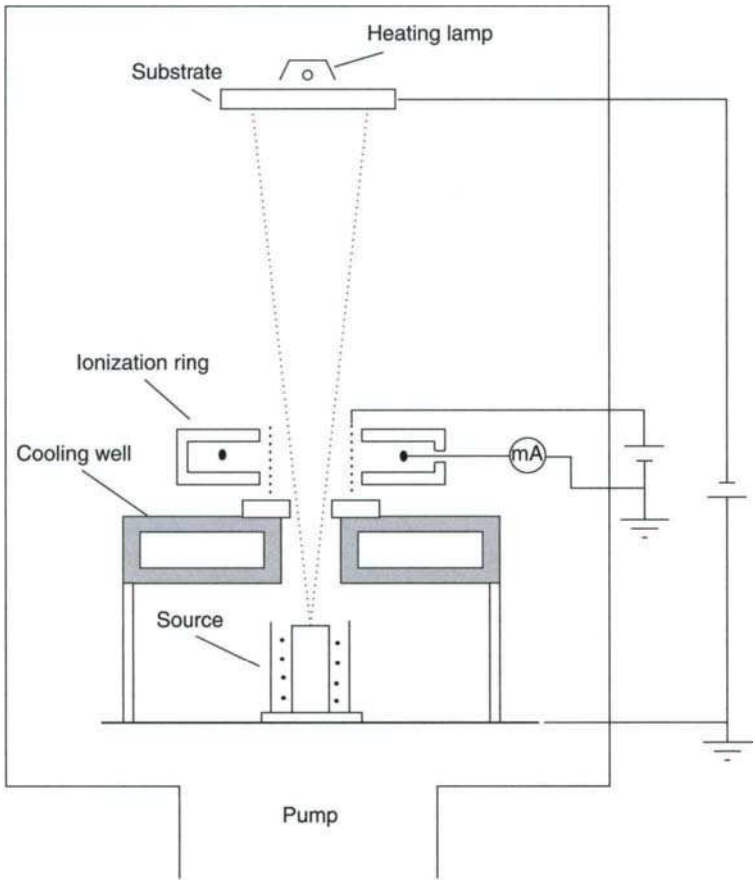

Figure 16 Diagram of ionized cluster deposition system. After J. S. Xie, Y. Zheng, and J. Y. Feng, *Nucl. Instrum. Methods B* 122, 239 (1997).

bonding structure, although the crystalline structure in films has been observed using a wide range of different techniques as is detailed later.

3.3. High Pressure Methods

A few reports have described attempts to make carbon nitride in crystalline form by similar methods as are used to make diamond or cubic boron nitride in bulk form, that is, by using high pressure (30 GPa) and temperature (2000–2500 K) in a laser-heated diamond cell [75], in which the chemical precursors were various forms of carbon such as graphite, amorphous carbon or fullerene, C_{60}, together with nitrogen, or by using shock compression at pressures greater than that in the range 60–250 GPa with organic precursors with a carbon–nitrogen ratio of approximately 3:4, the same as in stoichiometric β-C_3N_4. [76]

3.4. Electrolytic Methods

Reports have recently been made about deposition of CN_x:H films by electrodeposition on the anode in a cell in which the cathode was graphite with an organic electrolyte of acetonitrile or a solution of dicyandiamide in acetone [77, 78]. The mechanism of formation is believed to be because of polarization of adsorbed CN radicals on the anode surface. When the applied potential is high enough, the C–C bonds will break and the CN groups will then form carbon–nitride bonds on the substrate.

4. STRUCTURAL PROPERTIES OF CARBON NITRIDE

The behavior of the electrons in carbon nitride not only manifests itself as the overtly "electronic" properties such as band structure, optical absorption, and so forth but also implicitly influences the physical properties such as the interatomic bonding and hence the three-dimensional arrangement of the atoms in the material. It is therefore important to examine the structural properties of carbon nitride as a prelude to the consideration of those that are conventionally thought of as electronic. There are two means of identifying the bonding structure: (a) vibrational spectroscopy of the interatomic bonds and (b) electronic spectroscopy of the electrons emitted from the core and valence levels of the atoms as a result of some form of excitation.

The starting point is the electronic structure in the two constituent atoms, —carbon and nitrogen. The carbon atom in the ground state has a

$1s^2 2s^2 2p^2$configuration. It has an outer shell consisting of four electrons, two in the 2s shell and two electrons in the 2p shell. When forming physical structures, one of the 2s electrons is promoted into the vacant 2p orbital and these four electrons can then hybridize into different configurations. A combination of one s and three p orbitals forms four equivalent sp^3-hybridized bonds, each of which contains a single electron. These hybrid orbitals are directional and form a tetrahedral arrangement with a bond angle of 109.47° between any two. In a structure, the sp^3 orbitals form σ bonds, that is, they are radially symmetrical about the bond axis. A combination of one s and two p orbitals will form equivalent sp^2 bonds, which have a planar configuration with an angle of 120° between them; these are also σ bonds. The additional p electron can form a π bond in a direction perpendicular to the plane containing the σ bonds; this π bond is not symmetrical about the bond axis. Hybridization between one s and one p orbital will form two sp bonds that can form two σ bonds on opposite sides of the atom. In this case, the additional p electrons form two π bonds orthogonal to each other and to the σ bonds. In contrast, in the outer shell of nitrogen there are five electrons. The electron orbitals will also hybridize into various arrangements, but the additional electron compared with carbon will alter the bonding situation. For example, the bonds can form a planar trigonal structure with three σ bonds but because there are two additional electrons they will form a nonbonding "lone pair" and will not constitute π bonds. It is also conceivable that one of the electrons will form a π bond and the other will then be available for conduction, that is, the N atom will act as a donor (see Section 5.1.2.) or the atom will form four σ bonds with an extra electron available. The interatomic bonding affects both the electronic properties, as the σ and π bonding and the σ^* and π^* antibonding energy levels form the valence and conduction bands, and also the physical structure of the material, as the number and angle of the bonds determine the local atomic arrangement and hence the type of crystal that the material will tend to form.

4.1. Crystallography

The physical structure of carbon nitride materials can be determined most directly by crystallographic techniques. Transmission electron diffraction (TED) and X-ray diffraction (XRD) can show in the first place whether the material is crystalline or amorphous and then can determine the lattice spacing of the crystals and the crystallite size. Comparison with theoretical predictions can then elucidate the molecular structure of the material. However, most of the carbon nitride material that has been produced has been amorphous

in structure and therefore these techniques do not help in identifying the interatomic arrangements. In these cases, more indirect methods must be used.

4.2. Vibrational Spectroscopy

The phonon energies of the interatomic bonds in carbon nitride materials can be investigated by means of Raman and IR spectroscopy. In Raman spectroscopy, the photons in an incoming laser beam excite vibrations of the atoms. If there is a change in dipole moment as vibrations occur in the interatomic bond, the photon can lose (or gain) the amount of energy of the phonon of the vibration and the light is scattered with a frequency shift from the incoming radiation. Measurement of the frequency shifts between the incident radiation and the spectrum of the scattered radiation gives the vibrational frequencies of the bonds. In IR absorption spectrometry, the incoming electromagnetic radiation is directly absorbed by the vibrating atoms if the interatomic bond has a dipole moment in the plane of the incident electric field and the vibrational frequency of the bond matches the frequency of the radiation. The visibility of particular vibrations in both Raman and IR spectroscopy is governed by selection rules that determine whether they are active under the particular excitation. These rules are governed by crystal symmetry arguments; the details of the process and the derivation of the nomenclature is not considered here.

4.2.1. Crystalline Carbon Nitride

Theoretical calculations of the vibrational density of states of carbon nitride were carried out by Widany and coworkers [79] using a nonorthogonal tight-binding molecular dynamics simulation procedure based on density function. In this procedure, they considered a cluster of carbon and nitrogen atoms in the stoichiometric ratio 3:4 terminated by hydrogen at the outer boundaries and applied the process to four proposed crystal structures: an α phase and β phase analogous to the α- Si_3N_4 and β-Si_3N_4 structures, a cubic zinc blende structure (c-C_3N_4) with one carbon vacancy per unit cell, and a rhombohedral phase (r-C_3N_4) comparable to a graphite-like layered structure with carbon vacancies; all modifications have been proposed as stable or metastable crystals [11, 13, 17]. The results of these simulations are shown in Figure 17. From these data, the signatures for the α phases and β phases are seen to be very similar, whereas the c phases and r phases show behavior qualitatively similar to that shown by the cubic and hexagonal modifications of boron nitride that also have zinc blende and rhombohedral structures, respectively.

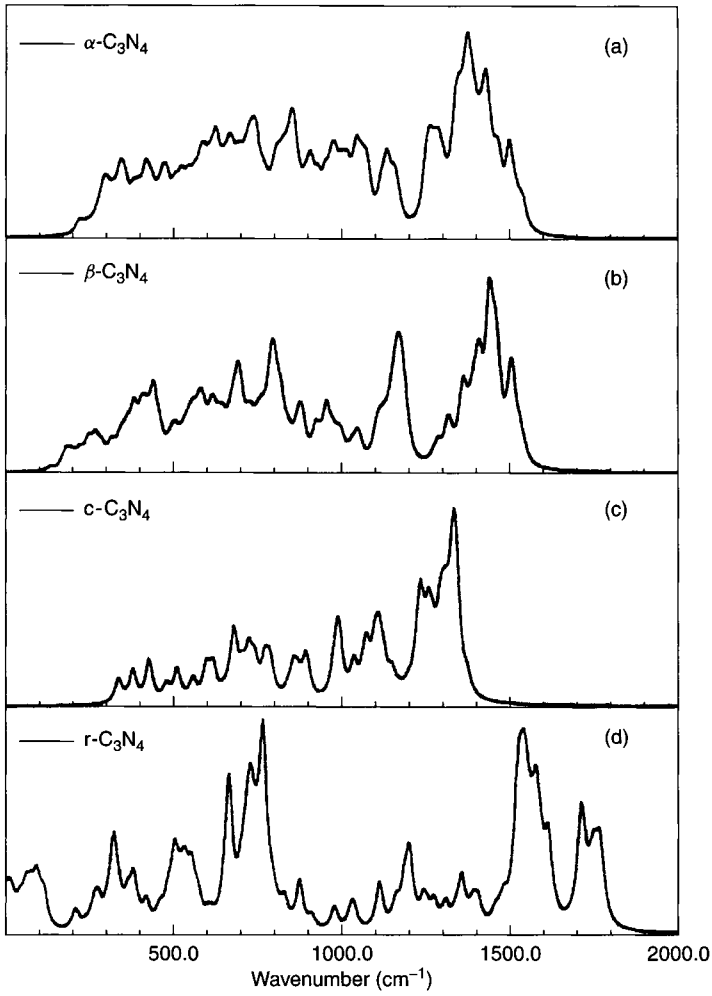

Figure 17 Calculated vibrational spectrum for (a) α-C_3N_4, (b) β-C_3N_4 (c) c-C_3N_4 and (d) r-C_3N_4. After J. Widnay, F. Weich, Th. Köhle, D. Porezag, and Th. Frauenheim, *Diamond Relat. Mater.* 5, 1031 (1996).

4.2.2. Amorphous Carbon Nitride

The behavior of amorphous carbon nitride (a-CN) can be compared with that of amorphous carbon (a-C) that in itself can be derived from the spectrum of disordered graphite. For graphite, the total zone center optic modes can be given as the following irreducible representation [80]

$$\Gamma = A_{2u} + 2B_{2g} + E_{1u} + 2E_{2g} \tag{3}$$

The A_{2u} and E_{1u} modes are IR active and are observed at 867 and 1588 cm^{-1}, respectively [81]. The E_{1u} and E_{2g} modes are Raman active [82]; the E_{2g} modes are observed at 42 and 1581 cm^{-1} [83]. The B_{2g} modes are inactive in both IR and Raman. The E-symmetry modes exhibit in-plane atomic displacements, whereas the A and B modes have out-of-plane displacements. For amorphous carbon, the E_{2g} mode is the so-called "G" band and the E_{1u} is only weakly IR active [84]. The "D" band that appears in the Raman signal at approximately 1360 cm^{-1} appears due to bond angle disorder in sp^2 graphitic domains or because of a lack of coherence between adjacent graphitic planes [85–87]; the existence of this band is taken as a sign of a degree of sp^3 bonding in the material. Figure 18 shows the typical Raman spectrum from an a-C film [88]. If there is no correlation between graphitic layers, the E_{1u} vibration does not appear in the IR spectrum because there is no perpendicular component to break its symmetry. As the sp^2 domain size increases, the intensity of the D-band relative to the G-band decreases [84, 85] and this has been used as a measure of the sp^3–sp^2 ratio. The peaks from a-C are broader and closer together than those for graphitic material, and this feature can also give an indication of how much of the film bonding structure is sp^3-type material [88]. The characteristic signature for diamond is the appearance of a sharp peak in the Raman spectrum at 1332 cm^{-1} as shown in Figure 19 [89]. The Raman signals from a-C are of low intensity and the IR spectrum is almost featureless; however, when nitrogen is introduced into the structure, the N atoms break the symmetry of the sp^2 domains and cause the Raman D and G bands to become more intense and also to become active in the IR, and the changes in intensity of these peaks can be used to give a measure of the amount of carbon–nitrogen bonding of these types.

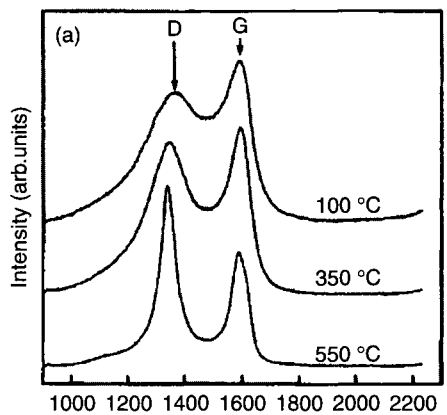

Figure 18 Raman spectrum for an amorphous carbon film showing the D and G peaks. After M. P. Johansson, E. Broitman, L. Hultman, and J. -E. Sundgren, *Phys. Rev. B* 59, 5162 (1999).

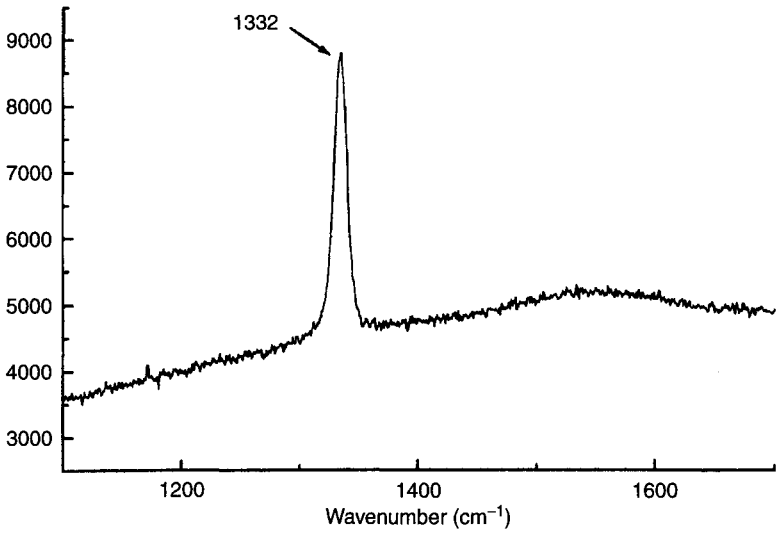

Figure 19 Raman spectrum for diamond film showing the characteristic 1332 cm^{-1} peak. After M. Schmitt, D. Paulmier, T. Le Huu, M. Elmansouri, A. Grabchenko, and A. G. Mamalis, *Thin Solid Films* 332, 124 (1998).

4.3. Electronic Spectroscopy

The energies of the core electron levels in carbon and nitrogen—the 1s states in this case—are affected by the local chemical environment of the atoms. The four most common methods used to investigate the core level electrons are X-ray photoelectron spectroscopy (XPS), Auger electron spectroscopy (AES), electron energy loss spectroscopy (EELS), and near-edge X-ray absorption fine structure (NEXAFS).

4.3.1. X-ray Photoelectron Spectroscopy

In XPS, the core electrons are ionized by X radiation, energy E_o, and they are emitted from the material with a kinetic energy E; therefore, the binding energy W_x of the electrons to the nucleus is given by

$$E = E_o - W_x - q\phi \tag{4}$$

where q is the magnitude of the electronic charge, ϕ is the work function of the material.

The binding energy, in general, increases with the electronegativity of the atoms attached to the one being observed because of the redistribution of charge, and this energy shift can then be used to attempt to identify the bonding structure.

4.3.2. Auger Electron Spectroscopy

In AES, Auger electrons are emitted by a three-body process in which a core electron is ionized by the incoming radiation, a higher-energy electron drops into the vacant state and in doing so releases enough energy to ionize another electron that has an energy characteristic of the atom. Auger electrons are also subject to chemical shifts, although their interpretation is more complex than that in XPS. The shape of the emission peaks is also affected by the local environment, but this process is again complex and very difficult to interpret. Attempts have been made to attribute the various features in the Auger emission peaks by a factor analysis process in which the line shapes for carbon nitride materials are reconstructed by linear combinations of the components that are expected to make up these materials and a consideration of the symmetries of the bonding structures [70].

4.3.3. Electron Energy Loss Spectroscopy

This technique analyzes the energy of electrons emitted from a material when it is irradiated by an electron beam. Two types of spectrum can be observed:

1. The low-loss spectrum in which the energy of the emitted electrons are reduced from the primary beam energy by the energy lost in exciting plasmon oscillations. Figure 20a [71] shows a typical example of this type of spectrum. There are two features that are normally to be observed: one at around 6 eV shift from the primary beam energy that is generally considered to be caused by to plasmon oscillations of the π electrons in graphitically bonded carbon atoms on sp^2 situations but may be caused by an asymmetric mode in which the σ and π electrons are oscillating out of phase with an amplitude determined largely by the π oscillations [69, 90, 91]. The other main feature is a peak at around 25 eV caused by bulk plasmon oscillations of the entire $\sigma + \pi$ valence band electrons [92, 93]. From the energy of the π-plasmon peak, E_p, the density of electrons in the valence band can be calculated according to the Drude model

$$E_p = \sqrt{\frac{h^2 q^2 n_e}{\pi m}} \tag{5}$$

where h is Planck's constant, q is the magnitude of the electronic charge, n_e is the density of valence electrons, and m is the electron mass. Following this equation, the density of the material, ρ, can be calculated from the density of valence electrons by the equation [33]

$$n_e = \rho \left(\frac{(n_C + x n_N)}{M_C + x M_N} \right) N_A \tag{6}$$

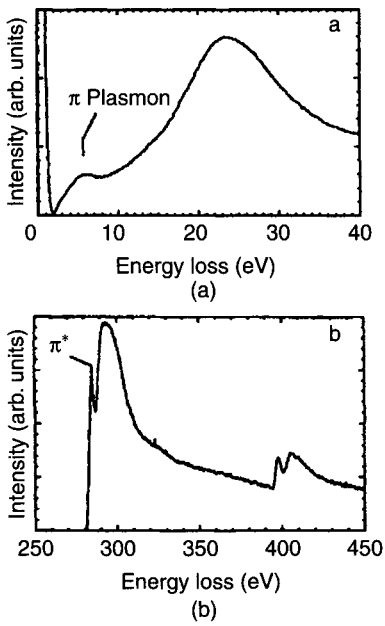

Figure 20 Typical EELS spectrum from carbon nitride (a) low-loss spectrum (b) K-shell energy loss spectrum. After K. J. Boyd, D. Marton, S. S. Todorov, A. H. Al-Bayati, J. Kulik, R. A. Zuhr, and J. W. Rabalais, *J. Vac. Sci. Technol.* 13, 2110 (1995).

where N_A is Avogadro's number, M_C, M_N are the atomic masses of C and N, respectively, n_C, n_N are the number of valence electrons in C and N, respectively, and x is the N–C ratio.

By comparing the size of these features with those observed in graphite and diamond that are totally sp^2 and sp^3 bonded, respectively, an estimate of the relative sp^2–sp^3 content can be obtained.

2. The spectrum caused by energy loss from the K electron shell of both nitrogen and carbon that tend to show a similar structure, comprising a more or less sharp peak caused by excitation of electrons into the π^* conduction band states and a broad peak or step caused by excitation into the σ^* states. From the relative sizes of these peaks and by comparison with the spectrum of graphite, an estimate of the sp^2–sp^3 ratio can be obtained. Figure 20b [70] shows an example of the typical signature from the K shell electrons.

4.3.4. Near-Edge X-ray Absorption Fine Structure (NEXAFS)

In this technique (also known as XANES), the film is irradiated by the intense radiation from a synchrotron X-ray source, and the electron yield or

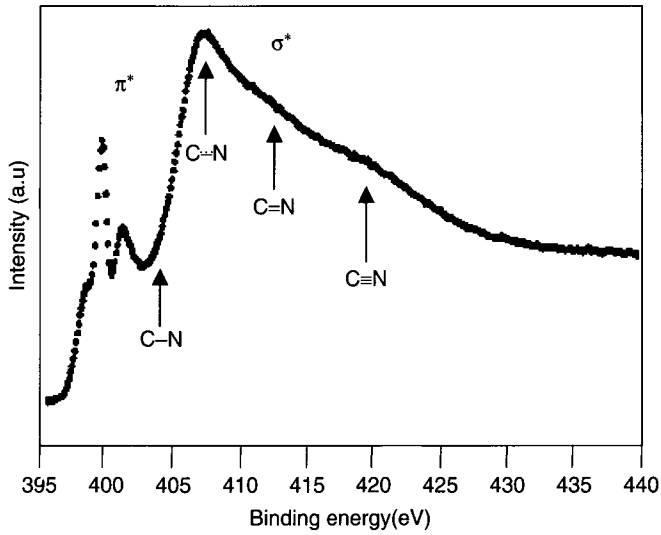

Figure 21 Typical NEXAFS spectrum from carbon nitride. After J. M. Ripalda, E. Román, N. Diaz, L. Galán, I. Montero, G. Comelli, A. Baraldi, S. Lizzit, A. Goldoni, and G. Paducci, *Phys. Rev. B* 60, R3705 (1999).

some other quantity proportional to X-ray absorption is measured as the X-ray photon energy is scanned near the binding energy of an atomic core level. The main feature is a peak resulting from transitions from the core level to free electron states above the Fermi level. The technique detects π bonding by the presence of a narrow peak a few eV below the main peak that is due to transitions from the 1s core level to the antibonding π^* molecular orbitals. The presence of σ bonding can also be seen by the presence of a broad peak just above the main peak resulting from transitions from the core levels to the σ^* antibonding orbitals. The main features of a NEXAFS signal from carbon nitride are shown in Figure 21 [94].

4.4. Observed Bonding Structures in Carbon Nitride

The vast majority of the carbon nitride material produced so far has been amorphous in nature. Therefore, vibrational and electronic spectroscopy are the techniques that have been applied to its analysis.

4.4.1. Fourier Transform Infrared (FTIR)

As mentioned in Section 4.3.1., for amorphous carbon, the IR absorption spectrum is relatively featureless because the various vibrations are not, or

are very weakly, IR-active in the normal region of measurement, that is, approximately 600 to 4000 cm^{-1}. However, as nitrogen is incorporated into the films, the intensity of the absorption band at 1350–1650 cm^{-1} (because of the sp^2 C=N bond stretching vibration) increases due to symmetry-breaking caused by nitrogen being introduced into the symmetrical carbon structure. The typical signature of a carbon nitride film with high nitrogen content is shown in Figure 22. The other main feature is a peak that occurs at approximately 2200 cm^{-1}, and this is normally ascribed to the C≡N stretching vibration. The intensity of the 1350–1650 cm^{-1} band increases with the nitrogen content of the films but does not increase linearly and tends to saturate at levels below the maximum nitrogen content. (The maximum nitrogen content according to most workers is approximately 40 atom %, regardless of the method of deposition. Some authors have claimed much higher levels, up to 80 atom %

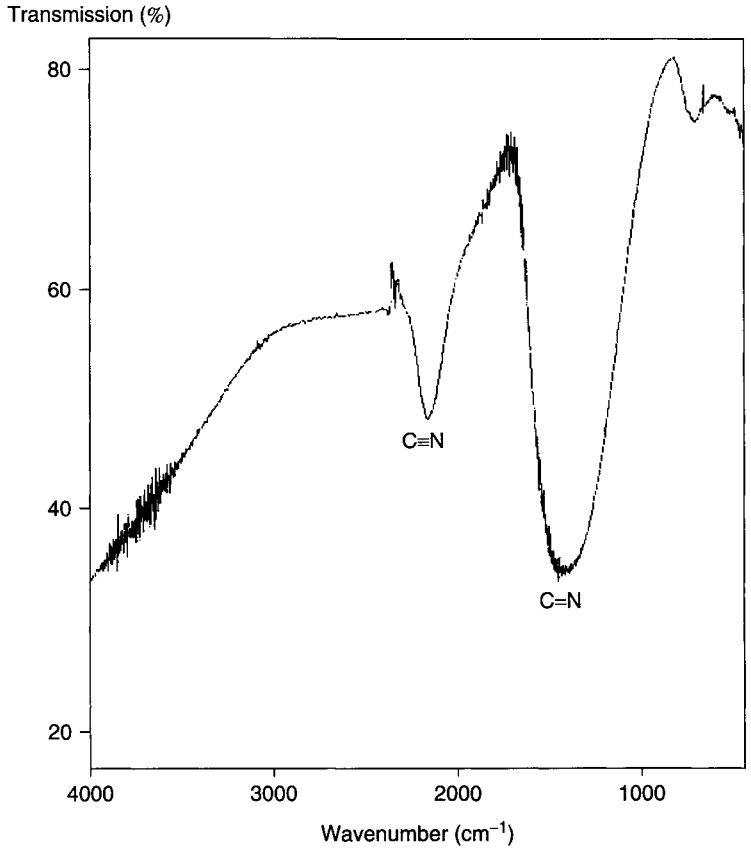

Figure 22 FTIR spectrum from film containing approximately 35% nitrogen.

but a carbon nitride structure with 80% nitrogen is difficult to envisage.) The absorption caused by the C–N sp^3 stretching vibration at approximately 1210 to 1265 cm^{-1} [75] overlaps with the main absorption band and is consequently difficult to observe in films that are a mixture of sp^2 and sp^3 material, although such a peak has been assigned in some cases [28, 95]. If the absorption caused by the C=N and C≡N vibrations saturates below the maximum of nitrogen content, the excess nitrogen must be forming some bonding structure that is either IR-inactive, weakly absorptive, or obscured by the existing absorption bands.

Particularly in films produced by PECVD in which hydrogen is a constituent of the precursor materials, absorption caused by the C–H and N–H vibrations at approximately 3000 $cm^{-1}$and approximately 3400 cm^{-1}, respectively, are often observed, showing that there is significant hydrogen content in the films. O–H bond absorption at approximately 3300 cm^{-1} can also be sometimes observed even in films grown under low-pressure condition, for example, by magnetron sputtering caused by incorporation of water from the adsorbed molecules on the chamber walls as a result of atmospheric exposure.

In materials showing a crystalline structure, there is still much disagreement about what characterizes the C–N sp^3 bond. A definite vibrational peak at 1388 cm^{-1} attributed to this mode has been observed [96], but the films contained a significant amount of oxygen and hydrogen and so it is not certain that this peak is due to C–N alone. In the work of Shi and coworkers [97], the IR spectrum has been compared with that calculated theoretically for crystalline forms of carbon nitride and the existence of a strong double peak at 853 and 888 cm^{-1} has been given as evidence of the β-C_3N_4 phase. It is clear, however, that a consensus has not yet been reached on these issues.

4.4.2. Raman Spectroscopy

The main observations in Raman spectroscopy in a-CN are very similar to those in FTIR. The D and G peaks are the most prominent features and there is relatively little variation in their size and position. The 2200 cm^{-1} C≡N peak is also observed for higher nitrogen contents, although it is not as prominent as in FTIR. A typical Raman spectrum is shown in Figure 23 [98]. Some workers have also identified a third Raman peak between the D and G peaks whose intensity increases at high levels of nitrogen content [99], and they have attributed this to a N=N stretching vibration similar to that which occurs in C–N=N–C ring structures [100], which will only become evident once there is enough nitrogen incorporated in the structure to make two nearest-neighbor nitrogen atoms likely.

As in IR spectroscopy, with crystalline material the identification of bonds resulting from the sp^3 C–N bond has been difficult. The spectrum of crystalline

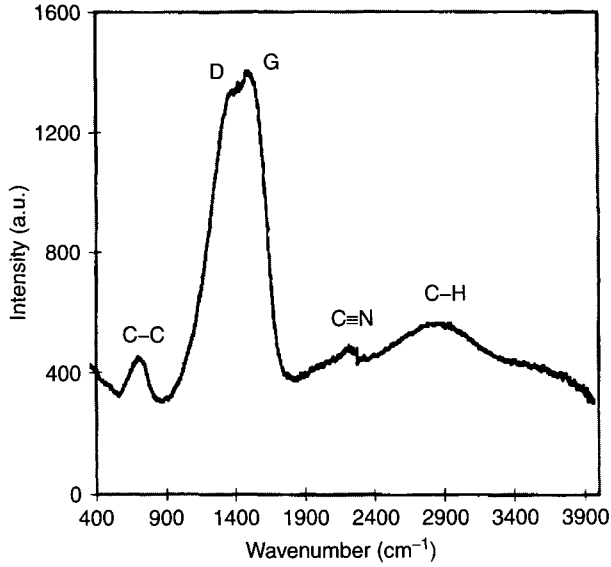

Figure 23 Typical Raman spectrum of an amorphous carbon nitride film. After A. K. M. S. Chowdhury, D. C. Cameron, and M. S. J. Hashmi, *Surf. Coat. Technol.* 112, 133 (1999).

films deposited on Ni substrates (to exclude the possibility of Si contamination) has indicated that the α- and β-C_3N_4 phases can be distinguished by comparison of the observed spectra with theoretical calculations as described in Section 4.2.1. [101].

4.4.3. Photoelectron Spectroscopy

There have been many reports on XPS studies of the behavior of the core-level electrons in carbon nitride material and the analysis of these is not straightforward; however, the analysis has been characterized by the varying interpretations that have been put on the components of the peaks obtained by curve fitting to the measured spectrum. The spectra are not characterized by single symmetrical peaks; according to most authors, four peaks are required to fit the C1s spectrum and three peaks are required for the N1s spectrum to get reasonable correspondence to the measured spectrum. Typical examples are shown in Figure 24. In most cases, the peaks are assigned to various bonding configurations by resource in comparison with studies on organic nitrogen–containing compounds such as those containing pyridine-like structures or by arguments from first-principles calculations of the binding

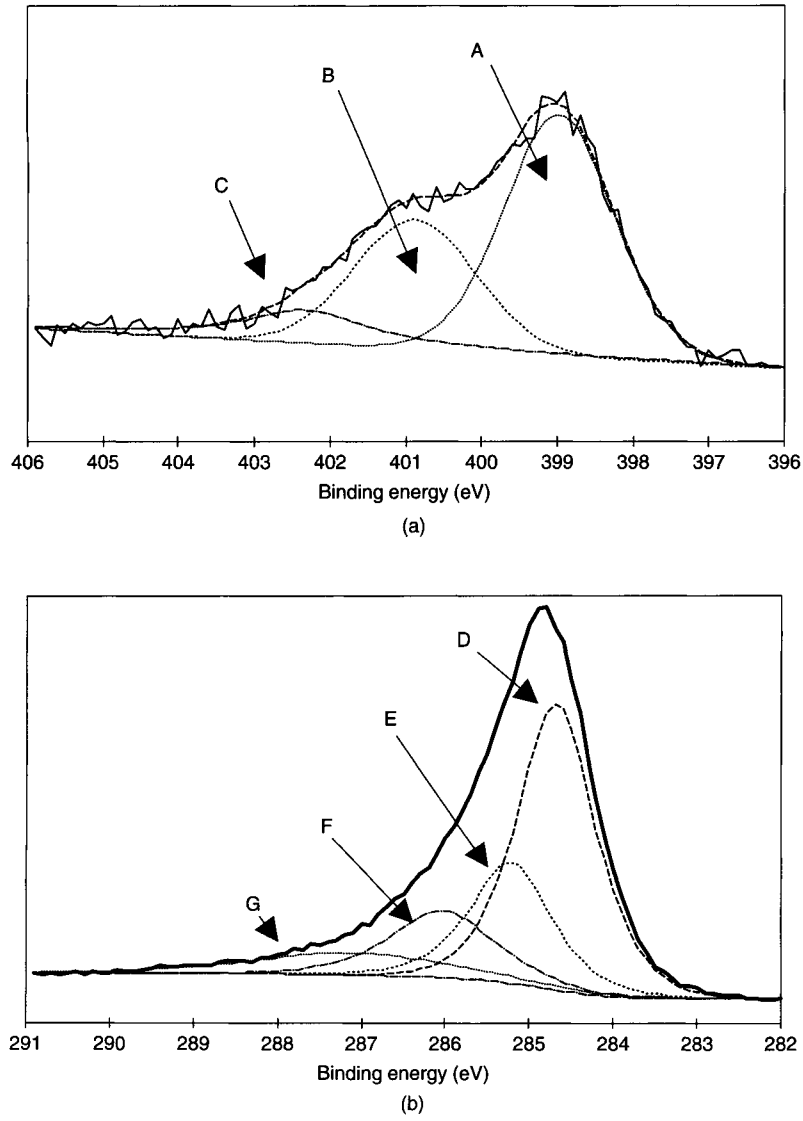

Figure 24 Typical XPS spectra from carbon nitride (a) N1s (b) C1s peaks.

energies. XPS studies have been notably carried out, for example, by Marton and coworkers [102] and Ronning and coworkers [103], who also reviewed the previous work in this area. By comparison of the spectra with organic materials, by consideration of the stoichiometry of the carbon nitride, and by observation of the evolution of peak position with nitrogen content, they

assigned the peaks as follows (see Fig. 24). For the N1s peak, the assignments are A: trigonally bonded nitrogen with three σ bonds and B: nitrogen bonded to two carbon atoms with two σ and one π bond. In addition, a third line C at higher binding energy is commonly assigned to a nitrogen–oxygen or nitrogen–nitrogen bond [e.g., 74, 102, 103]. In the C1s spectrum, the peaks were assigned as D: carbon–carbon bonding, E: tetrahedral carbon bonded to three carbon and one nitrogen atom, F: tetrahedral carbon bonded to two nitrogen atoms. They also considered that as the nitrogen content increases, sp^2 carbon–nitrogen bonds contribute to the D peak. The other small peak, labeled G, has been variously considered because of C–O and C≡N bonding [98, 102]. Other studies have compared the XPS behavior of films, as the nitrogen content changes due to growth conditions and postdeposition annealing with vibrational spectroscopy studies, and have attempted to correlate the results of each and have arrived at quite different assignments [98]. It is clear that there is still a significant amount of work to be carried out in this area to reconcile the opposing interpretations.

Information about the bonding structure can also be obtained by photoelectron spectroscopy of the valence band, but this is considered in Section 5. along with accounts of the valence band electronic states.

4.4.4. Electron Energy Loss Spectroscopy

The conclusions that have been drawn from EELS have, as is usually the case with carbon nitride, been rather contradictory. For example, the effects of the inclusion of nitrogen have ranged from very little [69] to an increase in the sp^2 content that begins at low levels of <0.1% N [93, 105–108]. The reason for this disagreement is probably because of the degree of sp^2 bonding in the original nitrogen-free films; those films in which the nitrogen-free material has a high degree of sp^3 bonding such as those produced by filtered cathodic arc evaporation [103, 106] may show a consequently greater effect with nitrogen incorporation than those in which there is already a significant amount of sp^2 -bonded material. However, a careful study of carbon nitride deposited by pulsed laser deposition [107] has shown that with highly sp^3-bonded amorphous carbon, the sp^3 content remained constant until the nitrogen content reached approximately 15%, at which point the sp^2 content increased rapidly together with a reduction in density consistent with this increase. This behavior was modeled by calculations on the atomic structure that showed similar changes in bonding at these levels of nitrogen content. The material density calculated from the plasmon energy measured by EELS has shown a reduction with N content [33], although recent measurements have suggested that for high films with high N concentration produced by DC magnetron sputtering, the density is unaffected by the N content [109]. Overall, the results of

EELS analysis support measurements made by the other analysis techniques in terms of the bonding structure of the films.

4.4.5. Near-Edge X-ray Absorption Fine Structure (NEXAFS)

Very few NEXAFS studies have been carried out on carbon nitride materials. One recent example has attempted to calculate the bond lengths from the position of the σ^* resonance [94]; the two features have been shown to be correlated [110]. These bond lengths have been assigned to sp-, sp^2-, or sp^3-bonded atoms by comparison of the bond lengths with those expected for the various C–N bonds.

5. ELECTRONIC AND OPTICAL PROPERTIES

The two types of carbon nitride structure, namely, the stoichiometric crystalline form that could be β-C_3N_4 or one of the other possible arrangements, or the amorphous form that contains variable amounts of nitrogen and may also contain hydrogen to a greater or lesser degree, depending on the method of deposition, should be considered separately. For the crystalline form, the starting point for investigation is a theoretical calculation of the band structure from an atomic orbital point of view, especially because electronic and optical characterization of the material has not yet been carried out because of the difficulties of obtaining it in sufficient quantities or with enough confidence in its structure and composition to draw sensible conclusions. For the amorphous material, obtaining stoichiometric material is not the issue, but the extremely wide variations that can occur in composition, structure, and impurity level makes it difficult to predict exactly what the characteristics of a "carbon nitride" film will be. However, a comparison of the band structure with that which is found in diamond-like carbon materials can be made.

This section is, divided for convenience, into two subsections dealing with (a) the "internal" electronic properties, that is, the band structure, particularly the details of the valence band states and (b) the "external" properties, that is, those that can be measured by some behavior of the film as part of an electronic or optical circuit. This distinction is somewhat artificial because both categories are interdependent and do overlap, but it is convenient for the purposes of description.

5.1. Internal Electronic and Optical Properties

5.1.1. Crystalline C_3N_4

β-C_3N_4 is the only structural modification for which detailed theoretical energy band calculations have so far been carried out. Liu and Cohen [10]

used a first-principles pseudopotential total-energy approach within a localized orbital formalism to calculate the ground state structural and electronic properties of β-C_3N_4 and β-Si_3N_4 (as a model to assess the validity of the results). The structural properties have already been referred to in Section 2. They calculated a total valence band width of 24.8 eV with a local density approximation (LDA) band gap of 3.2 eV. The valence band features that they calculated are broadly in agreement with those calculations that were carried out by Duan and coworkers [111], who calculated the energy bands using a first-principles "linear combination of muffin–tin orbital" method with the atomic sphere approximation (LMTO-ASA). In their calculations, they used a structure for β-C_3N_4 analogous to β-Si_3N_4 with the C–N bond length set to 1.47 Å, the empirical covalent radius as determined by Phillips [14]. The resulting band structure is shown in Figure 25 [111]. The top of the valence band is very flat along the MΓ axis, whereas the conduction band has a minimum near the Γ point. Therefore, β-C_3N_4 can be said to have a direct gap of magnitude 4.18 eV at the Γ point. The data are summarized in Table I. This value of energy gap as calculated by Liu and Cohen using a different approximation method [112] is between 3.2 eV [10] and 6.75 eV. Density of states (DOS) calculations shown in Figure 26 [111] show that near the conduction band edge the DOS is composed of all orbitals of both N and C and at the top of the valence band the DOS mainly consists of N2p orbitals. The band gap of β-C_3N_4 is less than that of β-Si_3N_4 because there are no d orbitals in the C valence shell, unlike Si.

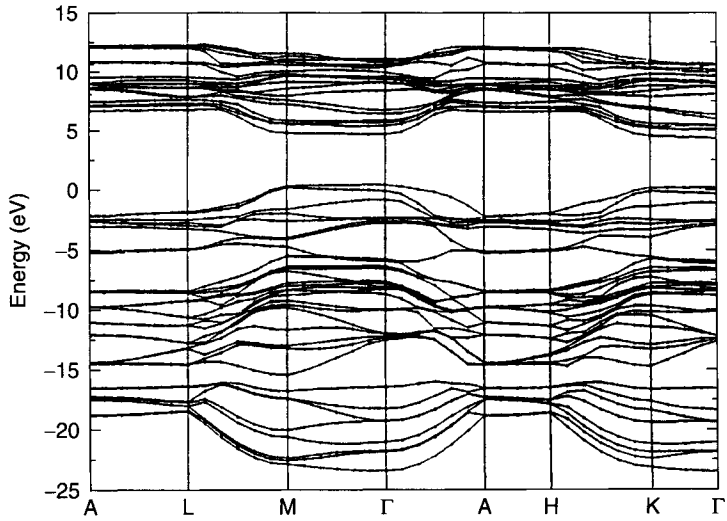

Figure 25 Calculated band structure for β-C_3N_4. After Y. Duan, H. Zhang, and X. Xie, *Phys. Status Solidi B* 200, 499 (1997).

Table I

Summary of Band Structure of β-C_3N_4 [111]

Band	Energy (eV)
Bottom of lowest valence band	4.18 (Γ)
Top of highest valence band	0 (Γ)
Bottom of 1st valence band	−23.38 (Γ)
1st valence band width	23.38
Band gap	4.18

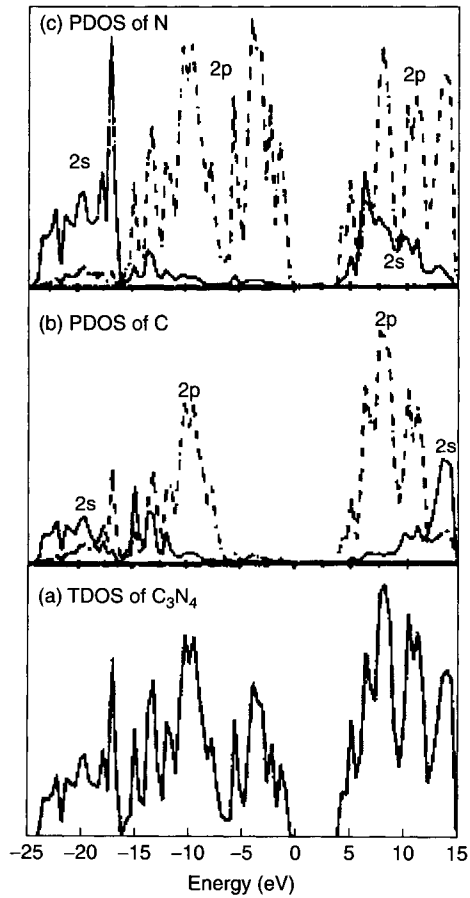

Figure 26 Density of states calculations for β-C_3N_4. After Y. Duan, H. Zhang, and X. Xie, *Phys. Status Solidi B* 200, 499 (1997).

To date, there have been no optical measurements on crystalline carbon nitride films that would support or contradict these calculations.

5.1.2. Amorphous Carbon Nitride

5.1.2.1. Valence Band Structure

The electronic properties of amorphous carbon nitride are critically dependent on the bonding nature of the materials as would be expected. Thus, the method of preparation has a profound influence. In particular the sp^3-sp^2 bonding ratio in the films is important because it affects the number of electrons in σ-and π-bond configurations. In the case of carbon films containing no nitrogen, diamond has a band gap of 5.3 eV, whereas in graphite there is an overlap between the conduction and valence bands. A diagram of the calculated band structures is shown in Figure 27 [114]. In undoped amorphous carbon films, a situation somewhat analogous to a mixture of the two pertains. The σ-bonding states and σ^* antibonding states from the sp^2 and sp^3 bonds form bands on either side of the Fermi level with a separation between them of 5–6 eV [115]. The π and π^* bonding and antibonding states from the sp^2 bonds give rise to valence and conduction bands with a smaller separation than the $\sigma-\sigma^*$ bands. Therefore, the band gap is largely controlled by these states. Theoretical modeling has suggested that the size of the band gap and the number of states within it is dependent not only on the sp^3-sp^2 bonding ratio but also on the organization of the sp^2 material into clusters [114]. Tetrahedral amorphous carbon or ta-C, both hydrogen-free and that containing hydrogen, which has a high proportion of sp^3 bonds and consequently relatively few sp^2 clusters, has been found to have p-type doping by measurement of the thermoelectric power [116, 117].

When the films contain nitrogen, doping may or may not occur depending on how the nitrogen atom is bonded to the neighboring carbon atoms. The five valence electrons of nitrogen (two 2s and three 2p electrons) can have a number of possible configurations and whether a configuration is bonding or nonbonding will depend on whether the arrangement results in the existence of an unpaired electron. A description of these possible configurations has been given by Robertson and Davis [118] and Silva and coworkers [63]. A diagram of these is shown in Figure 28. In this diagram, pairs of valence electrons either form bonds that are shown as a line or in a "lone pair" configuration shown as two dots. Neither of these arrangements contributes to doping. Doping can only take place if there is an unpaired electron, shown as a single dot. In (a), which is the situation when N is bonded to three carbon atoms in a trigonal arrangement as would be the case in β-C_3N_4 (note that the bond angles shown in Figure 28 are only schematic and are not meant to represent the real situation, for example, in β-C_3N_4, the nitrogen bond angles would

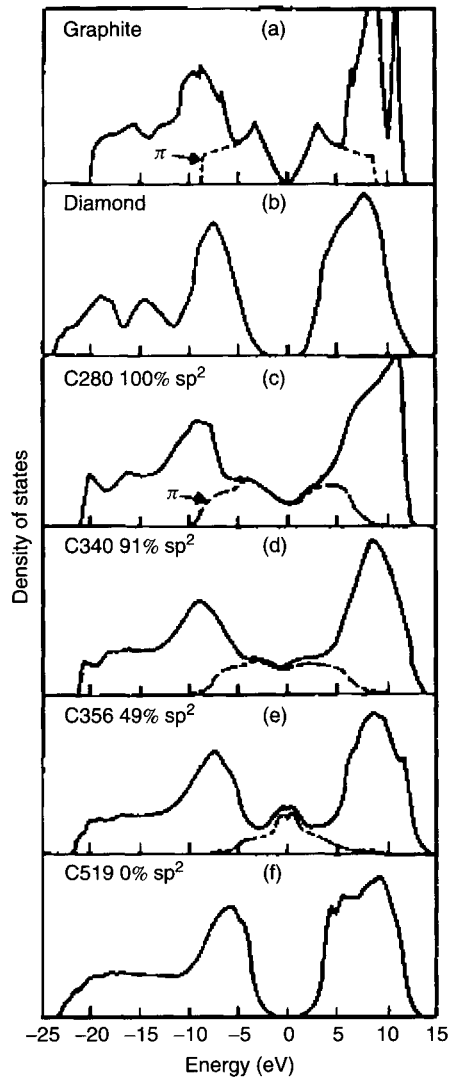

Figure 27 Calculated band structures for various forms of carbon film. After J. Robertson and E. P. O'Reilly, *Phys. Rev. B* 35, 2946 (1987).

be 120° in a planar arrangement), the N atom forms three σ bonds and the remaining electrons form a lone pair. The N atom could also possibly form four σ bonds that would leave one electron available for doping (b). In (c), this unpaired electron could be transferred to an adjacent C atom to form a N^+/C^- defect pair. The nitrogen can form π and σ bonds. If the N substitutes

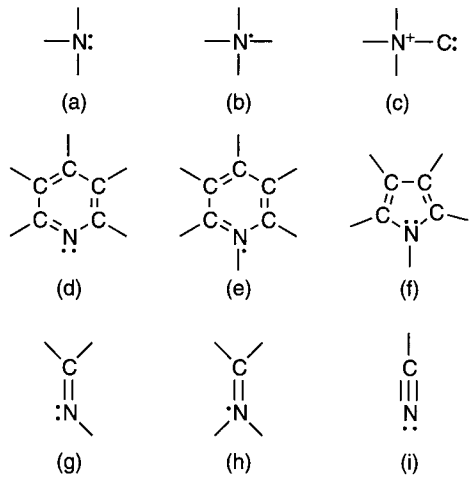

Figure 28 Possible bonding configurations of nitrogen in a carbon network. After S. R. P. Silva, J. Robertson, G. A. J. Amaratunga, B. Rafferty, L. M. Brown, J. Schwan, D. F. Franceshini, and G. Mariotto, *J. Appl. Phys.* 81, 2626 (1997).

for C in a ring structure, which is possible because a-C contains clusters of sp^2 material, there are again doping and nondoping configurations. If the ring has six members, the N could substitute as in (d) where two σ and one π bond is formed with the two adjacent C atoms and the other two electrons form a nondoping lone pair as in pyridine. If the N bonds with three adjacent atoms by means of three σ and one π bond, there will be one remaining electron in an antibonding π^* state. If the N is part of a five-membered ring, then it is in a situation similar to (a) and forms a nondoping lone pair. There are also linear chain bonding possibilities. In (g) and (h), it can be seen that the N atom is in a similar local situation to (d) and (e) giving a nondoping and doping arrangement, respectively. In situations in which the N is in a triply bonded state, it is not part of a continuing chain or ring structure; then the nonbonding electrons will form a lone pair (i).

The valence band structure can be observed by excitation of electrons from valence band states by X-rays in XPS or by UV radiation in UPS. The results given by the two methods are rather different because in the case of X-rays the valence band electrons are emitted with high energy and are not affected by the conduction band, whereas in UPS, the measured intensity is the result of a convolution of the conduction and the valence band states. The electrons also have different absorption cross sections for the different radiation energies [119]. Thus, the intensity of the peaks from the two methods cannot be compared directly. However, both techniques show common features resulting from the valence band states. Assignments of the position of various peaks

in energy near the Fermi level in carbon nitride material have been made by theoretical calculations using an ab initio pseudopotential technique based on the Hartree-Fock theory [120, 121]. Bands located at approximately 3.5 eV and approximately 7.7 eV are associated with C–C π and σ bonds. A band at approximately 4.5 eV is attributed to lone pair electrons from sp^2-hybridized nitrogen, whereas at approximately 7 eV is a feature caused by C2p and N2p electrons in aromatic rings containing at least one substitutional nitrogen atom. A band at approximately 9.5 eV is also because of C2p and N2p electrons but in σ bonds rather than in π bonds. At deeper levels, peaks caused by sp electrons at 15–20 eV and s electrons at approximately 25 eV can be assigned by analogy with various forms of carbon [93]. A UPS valence band spectrum illustrating these bands is shown in Figure 29 [122].

For PECVD films grown with significant hydrogen concentration (up to ~14%), at relatively low N (<10%) incorporation levels, the effect of the N is to increase the graphitization of the material with an increase in the size of the sp^2 domains and the replacement of carbon by nitrogen in the aromatic ring structure. The increased incorporation of nitrogen is accompanied by an increase in the band intensity because of the lone pair electrons of nitrogen, although this same feature has been ascribed to a nitrogen defect band by

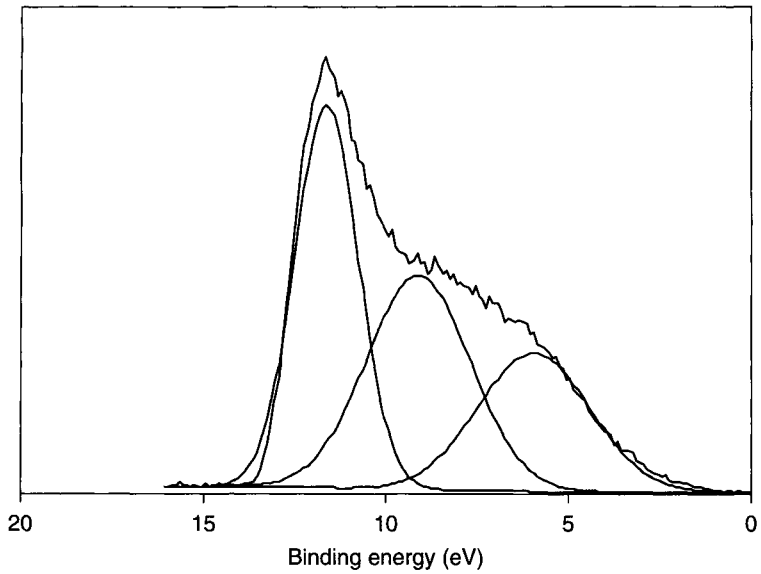

Figure 29 UPS spectrum from carbon nitride film. After M. A. Monclus, D. C. Cameron, A. K. M. S. Chowdhury, R. Barklie, and M. Collins; Presented at Asian-European Conference on Plasma Surface Engineering, (AEPSE 99), Beijing, 22–25th Sept. 1999.

comparison with theoretical calculations [118]. This increase in the density of the bands is accompanied by the reduction in optical gap that has been previously mentioned. With very low nitrogen incorporation (<7%), some authors have observed a reduction in width of the π-bonding states causing the optical gap to increase because of a more relaxed bonding structure with less strain and distortion. Studies on the effect of hydrogen incorporation confirm that the π-state intensity reduces and the optical gap increases and also that the C–N π bonds are partly replaced by C–H and N–H bonds as might be expected.

XPS valence band spectra for hydrogen-free films deposited by magnetron sputtering show that for 0% N atom%, the shallow valence band is dominated by the σ bands at approximately 10 eV with a smaller π component at approximately 5 eV. As the nitrogen content is increased, the π peaks become relatively larger than the σ peak because of the increased sp^2 content, consistent with the results mentioned earlier. However, with further increase in nitrogen content (~35% atom%), the σ peak again starts to dominate, suggesting that the sp^3 content increases again [122]. At deeper levels the sp mixed band at approximately 20 eV is the major peak. (This apparent change in bonding structure is not accompanied by any density change and the increase of sp^3 bonding with high nitrogen content is in contrast to all other studies.)

5.1.2.2. *Optical Absorption*

The optical absorption edges of amorphous semiconductors such as silicon that can be characterized by an optical gap are most often analyzed using two formulas. At photon energies above the optical gap, the absorption behaves according to the Tauc formula [123].

$$(\omega\alpha)^{1/2} \propto \hbar\omega - E_T \tag{7}$$

where E_T is known as the *Tauc gap*.

This relationship assumes that both the conduction and valence bands are continuous with a parabolic DOS function. Below the optical gap, the absorption behaves according to the Urbach formula [124], that is,

$$\alpha \propto \exp\left(\frac{\hbar\omega - \hbar\omega_0}{E_0}\right) \tag{8}$$

where $\hbar\omega$ is called the *Urbach parameter* and E_0 represents the width of the absorption edge.

For this relationship to hold, the electrons must move in a Gaussian-correlated random potential profile [125]. With DLC films, the optical gap determined from the Tauc formula scan range from almost 0 to 5 eV depending on the deposition parameters [126] that produce major variations in, for

example, the sp^3-sp^2 ratio. However, in a-C there is no clear distinction between areas of Tauc and Urbach behavior; the parameters obtained have not shown consistency, and their physical significance has not been clear. The basic assumptions behind these models are not valid in the case of a-C, the structure of which has been considered to be nonhomogeneous and consists of clusters of sp^2-bonded material in a sp^3-bonded skeleton [114] or with even more disorder than this. This model implies that there are significant fluctuations in the band gap within the material leading to localized states caused by electron confinement within the clusters [127]. Near-edge transitions take place between these localized states in the sp^2 clusters rather than between continuous bands. Also, because of the large band gap, fluctuations at the site of the sp^2 clusters invalidates the assumptions of the Urbach model. A more physically based quantum well model was developed [128] to take account of these problems. However, the Tauc band gap, because of the ease with which it can be measured, is still widely used as an indication of the optical gap and a means of comparison between different films. The photon energy at which the optical absorption coefficient has a value of 10^4 cm^{-1}, E_{04}, is also used as a measure of the optical gap.

The effects of low levels of nitrogen incorporation into films with an (undoped) sp^3-sp^2 ratio of approximately 0.2–0.35 that can perhaps approximate to a "doping" situation rather than a structural rearrangement have shown that the optical gap, estimated from Tauc plots or from the E_{04} level, initially increases with nitrogen concentration reaching a peak at approximately 7% [129] or approximately 4% [130], although there is a large amount of scatter in the data, particularly in [130]. These results are shown in Figure 30. The films were produced by different methods; RF-PECVD in the case of [129] and plasma beam deposition in the case of [130]. Both results described films containing an appreciable amount of hydrogen, 19% and 14%, respectively, which generally has the effect of increasing the sp^3-sp^2 ratio. This is demonstrated by measurements on ion beam–deposited films in which the amount of hydrogen was altered, whereas the nitrogen content was kept constant [131]. These results showed that the hydrogen had a dramatic effect on the optical gap. These data are plotted in Figure 31. Notwithstanding the reservations regarding the validity of the Urbach model, the Urbach energy has been measured as a function of nitrogen flow during plasma beam deposition [130]. For low flows (and similarly low nitrogen content in the films), the Urbach energy remains similar to its level in carbon films consistent with a high level of defects of approximately 10^{20} cm^{-3}. At larger flows, the energy becomes larger, consistent with the widening of the band tail states, causing the decrease in the optical gap shown in Figure 30.

For films deposited under mainly hydrogen-free conditions, for example, by either ion beam deposition (IBD) [132], laser ablation (LA) [133], or DC

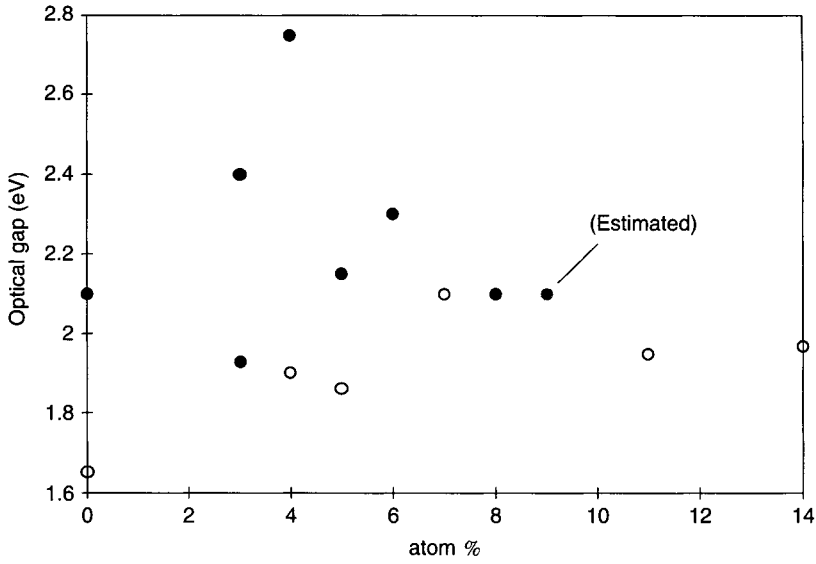

Figure 30 Optical gap as a function of nitrogen content, [extracted from S. R. P. Silva, B. Rafferty, G. A. J. Amaratunga, J. Schwan, D. F. Franceschini, and L. M. Brown, *Diamond Relat. Mater.* 5, 401 (1996)], [extracted from J. Schwan, V. Batori, S. Ulrich, H. Erhardt, and S. R. P. Silva, *J. Appl. Phys.* 84, 2071 (1998).

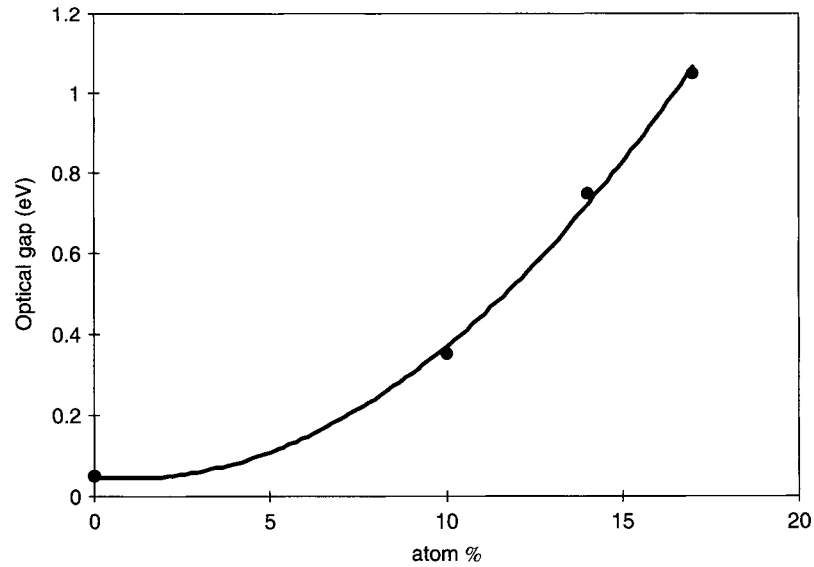

Figure 31 Variation of optical gap with hydrogen concentration. After P. Hammer, N. M. Victoria, and F. Alvarez, *J. Vac. Sci. Technol., A* 16, 2941 (1998).

magnetron sputtering [137], the optical gap is much lower because of the larger sp^2 content; in the hydrogen containing films, the H atoms can terminate some carbon bonds and promote the sp^3 configuration. The behavior with increased N incorporation can, however, be quite contradictory. A reduction in Tauc gap from approximately 0.6 eV for nitrogen-free films to approximately 0 eV has been reported [113, 132] and this could be ascribed to broadening of the $\pi-\pi^*$ bands by increased sp^2 cluster size, whereas the results reported by Monclus and coworkers [134] show that initial incorporation of nitrogen dramatically reduces the Tauc gap from approximately 0.5 eV for carbon films to approximately 0 eV for 25% content and then increases the optical gap with further nitrogen incorporation. Lu and coworkers [133] also found an increase in optical gap with nitrogen content. If the sp^3-sp^2 ratio is very high as in the case of films deposited by FCA deposition, FCA the band gap can be very high. In contrast to the behavior of hydrogen-containing films, Chen and coworkers [135] found that the optical gap initially reduced with nitrogen content then increased reaching a maximum of 3.8 eV at approximately 24% content, whereas Chen and coworkers [136] used the same process and found a decrease in optical gap from 2.5 to 1.6 eV under the same circumstances. This inconsistency in the characteristics points out the fact that without knowing the structure of the films, in some detail it is extremely difficult to arrive at any general conclusion about the effect that nitrogen doping has.

5.1.2.3. Refractive Index

There are rather few measurements reported of the refractive index of carbon nitride films and, as is common with this material, they are contradictory. It is sometimes found that the refractive index n of hydrogen-free films reduces as nitrogen content increases and Wang [113] attributed this to nitrogen having a stabilizing effect on the sp^3 bonds because in carbon films, both with and without hydrogen, it has been reported that the refractive index increases as the sp^3-sp^2 decreases [137, 138]. However, their results are complicated by the fact that the nitrogen was reduced by increased energy of ion bombardment. Therefore, it is impossible to separate the two effects. The same reduction in refractive index with nitrogen content has been ascribed to exactly the opposite behavior that is, an increase in the sp^2 fraction and a reduction in film density [139]. Most authors who have measured the refractive index have found that n increased as the nitrogen content increased [132, 133], again probably because of the increased graphitization that takes place (at least with moderate levels of nitrogen content). A linear dependency of n with $h\nu$ was also found, in which n was lower at higher photon energies; however, other results on RF magnetron–sputtered films have shown an increase in refractive index with photon energy [140]. Extinction coefficient, k, has been found to vary widely mainly because of the sp^2 content, as films can vary from transparent to black

depending on the deposition parameters. An increase in n after annealing of films deposited by the pulse plasma process [141, 142] has been reported, again probably because of graphitization.

5.1.2.4. *Conductivity*

The electrical conductivity of the films also varies over a very wide range, depending to a large extent on the sp^3-sp^2 ratio as influenced by the deposition process, and the activation energy of the conductivity can also show behavior ranging from the semiconducting to the semimetallic. Values ranging from $>10^{-14}$ to 1 $(\Omega\ \text{cm})^{-1}$ have been measured, [143]. Again, this measurement is largely a reflection of the degree of graphitization in the films. The predicted and measured conductivity of ta-C films with a high sp^3-sp^2 ratio is p-type [117, 142, 145]; in contrast, films with a lower sp^3-sp^2 ratio produced by magnetron sputtering have been found to be n-type [134]. If there exist a significant number of trapping states within the band gap, the thermal activation energy of the conductivity gives a measure of the separation between the Fermi level and the conduction band edge. Silva and coworkers [129] showed that with increase in nitrogen concentration, the activation energy increased from a value of 0.5 eV for undoped films to 0.9 eV for films containing 7% of nitrogen followed by a reduction to 0.45 eV with higher doping levels. They ascribed this change in activation energy to a movement of the Fermi level upward in the band gap with a consequent change from the p-type undoped state to an n-type doped condition but gave no data on the magnitude of the conductivity. However, as mentioned earlier, they also found an increase in optical gap of 0.4 eV over 0 to 7% doping; so the apparent doping effect may have been because of the widening of the gap. Plasma beam and ion beam deposition by the same group [130] have been found to give quite different relationships between conductivity and Tauc gap; in plasma beam deposition, the conductivity and optical gap are relatively high (10^{-5} to 10^{-3} $(\Omega\ \text{cm})^{-1}$ and 1.5–2.0 eV, respectively) whereas in PECVD, the optical gap changes from 0.5 to 1.5 eV as the conductivity ranges from 10^{-3} to 10^{-14} $(\Omega.\text{cm})^{-1}$. They found that the activation energy decreased from 0.27 to 0.18 eV as nitrogen content rose from 0 to approximately 8%, indicating only a slight movement of the Fermi level through the gap, although similar to the results of [129], the optical gap varied by 0.6 eV over the same range. Monclus and coworkers [134], who investigated films with a much higher level of nitrogen content and no hydrogen also found that the activation energy increased with nitrogen concentration and that the behavior changed from metallic for nitrogen-free films to semiconducting once an appreciable amount of nitrogen was incorporated, indicating a shift in the Fermi level away from the conduction band.

There have been very few measures of the mobility of the charge carriers in these materials. Schwan and coworkers [130] found that the mobility of the electrons increased from an unmeasurable quantity for nitrogen-free CN:H films to approximately 10 $cm^2V^{-1}s^{-1}$ with a maximum nitrogen concentration of approximately 8%.

5.1.2.5. Electron Density

Measurements of the density of unbonded electrons can be carried out using electron spin resonance (ESR), which gives the density of unpaired electron spins in the sample. Once more there is much variation between the results from different deposition processes. Those with significant hydrogen content show a reduction in spin density with moderate nitrogen content from the mid-10^{20} cm^{-3} range [129, 130] and from the mid-10^{19} cm^{-3} range [94], although the amount of variation is different in each case (Fig. 32). Nonhydrogenated

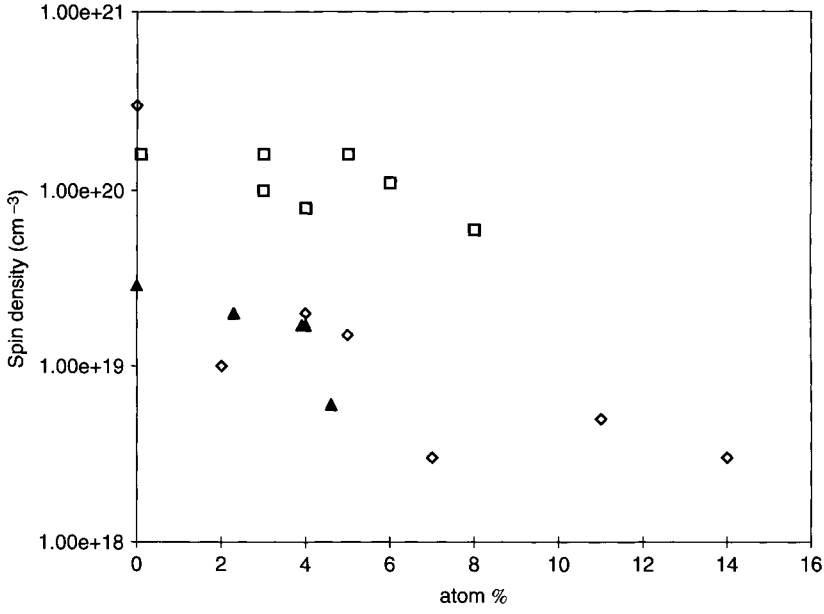

Figure 32 Variation of spin density with nitrogen content for hydrogenated films ◇ [After S. R. P. Silva, B. Rafferty, G. A. J. Amaratunga, J. Schwan, D. F. Franceschini, and L. M. Brown, *Diamond Relat. Mater.* 5, 401 (1996). □ [After J. Schwan, V. Batori, S. Ulrich, H. Erhardt, and S. R. P. Silva, *J. Appl. Phys.* 84, 2071 (1998), ▲ [After S. Bhattacharya, C. Vallee, C. Cardinand, O. Chauvet, and G. Turban, *J. Appl. Phys.* 85, 2162 (1999).

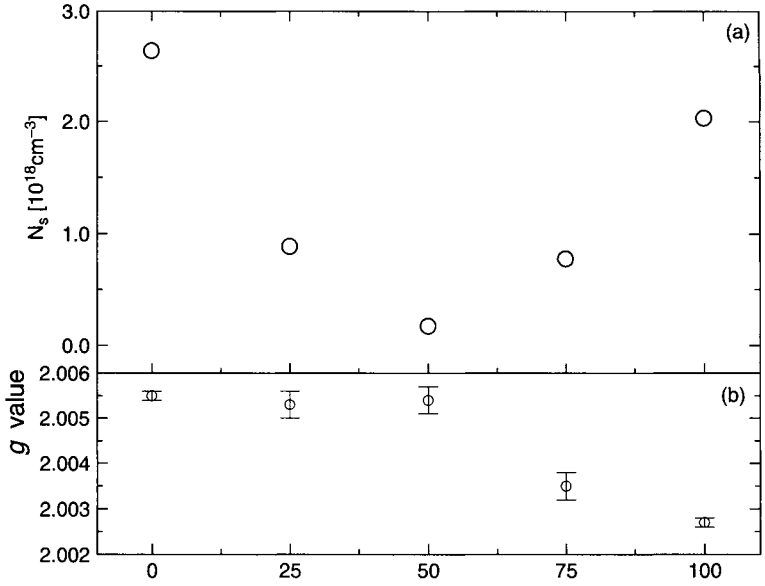

Figure 33 Variation of spin density and g value with nitrogen partial pressure during deposition for sputtered carbon nitride films. After M. A. Monclus, D. C. Cameron, A. K. M. S. Chowdhury, R. Barklie, and M. Collins, *Surf. Coat Technol.* 131, 488 (2000).

films show a much lower spin density in the mid-10^{18} cm^{-3} range for undoped films, even though there is no hydrogen present to passivate the unpaired electrons. This lower value may, however, be because of the higher graphitic content of these films [129]. It was also shown that the spin density increased again once the nitrogen content reached approximately 25%; at the same time the g value that was constant at approximately 2.0055 for lower nitrogen content reduced to 2.003 for the highest nitrogen content as shown in Figure 33. A significant reduction in spin density was also found as the magnitude of the (negative) substrate bias was increased during deposition along with a reduction in resistivity. This could not be explained by an increase in graphitization because valence band spectroscopy also showed reductions in the π-state density during the same process [146].

5.2. "External" Electronic and Optical Properties

5.2.1. Field Emission

The main interest in the electrical properties of carbon nitride films have been in their field emission properties for use in flat panel cold cathode field emission displays. To extract sufficient electrons from materials with relatively

high work functions such as Mo or W, cathodes with sharp tips have been used to locally enhance the electric field [147]. This approach necessitates complex and expensive patterning and etching processes and the resulting structures are not mechanically robust. An alternative approach is to use a flat cathode and to obtain the high electron emission by using a coating on the cathode with a low work function that requires less electric field to excite electrons to the vacuum level. Carbon-based coatings such as diamond [148, 149], nitrogen-doped diamond [150], and various forms of diamond-like carbon [151, 152] have attracted attention recently because of their chemical inertness, high thermal conductivity, low work function, and low or even negative electron affinity, and this means that any electron that reaches the conduction band of the material will be emitted from the surface. There have also been attempts to combine both approaches by patterning the carbon layer into cylindrical emitter tips by reactive ion etching of DLC films [153]. Carbon nitride films have been investigated because of the possibility of increasing the conductivity of the films as a result of the nitrogen incorporation as discussed in Section 5.1.2.4. A number of techniques have been used to deposit the carbon nitride films: for example, filtered cathodic arc deposition [154], helical resonator PECVD [155], sputtering [156], and microwave ECR PECVD [157]. The sp^3-sp^2 ratio is, however, quite different for the various deposition processes and this has a significant effect on the results that have been obtained, as might be expected. Carbon nitride films have also been deposited on molybdenum needles to enhance their emissivity [158]. The typical method of observing the field emission is by causing the emitted electrons to strike a transparent electrode in high vacuum and observing the resulting luminescence [159]. A schematic diagram of a typical arrangement is shown in Figure 34. Other methods are to measure the field emission current as a function of applied voltage, particularly if emission can be confined to small area such as a sharp tip or by using a scanning tunnelling microscope to map the field emission current density of an area of the substrate. According to the Fowler-Nordheim (FN) theory, the current density caused by field emission obeys a relation as follows [160]

$$J = A(\beta E)^2 \exp\left(-\frac{B\phi^{3/2}}{\beta E}\right) \tag{9}$$

where J is the current density in $A.m^{-2}$, ϕ is the work function in eV, E is the electric field in $V{\cdot}m^{-1}$, β is a field enhancement factor that takes account of the increased emission at sharp corners, $A = 1.4 \times 10^{-2}$, and $B = 6.8 \times 10^9$.

In theory, from the slope of a graph of $\log(I/E^2)$ vs $(1/E)$, the work function of the film material can be calculated. However, this calculation assumes a knowledge of the field enhancement factor, β. Even for flat films it is not likely to have the value one, because emission tends to come preferentially

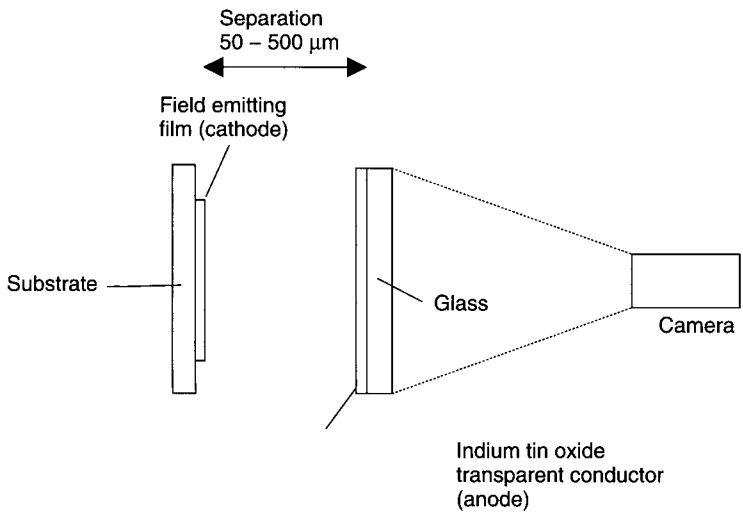

Figure 34 Schematic diagram of system for observing field emission.

from inhomogeneities in the film such as domain boundaries or irregularities in the surface [153].

Emission is found to be enhanced where the conductivity of the film is higher and the sp^2 concentration in the film is increased. This observation appears to be true for high-resistivity films with a high sp^3 content produced by FCA deposition [159] and also for low-resistivity films with up to an estimated 95% sp^2 ratio [160] produced by sputtering. It is also true for hydrogenated CN films. In all cases, treatment that increases the sp^2 content in the films by laser irradiation, thermal annealing, or nitrogen incorporation enhanced the field emission current and lowered the field emission threshold. The precise role of nitrogen in the field emission process is not clear. It may be having little effect on its own account—its usefulness may be as a method of controllably increasing the sp^2 content or altering the sp^2 domain sizes. This model is contradicted by the interpretation of Cheah and coworkers [156] on nitrogen-doped FCA material deposited under conditions in which nitrogen-free samples have sp^3 fractions up to 88% [160] (although it was not clear what the sp^3 content in the N-doped films was). These results suggested that enhanced emission was produced from sp^3-rich clusters in the films having lower electron affinity than the surrounding sp^2-rich boundaries.

Again the striking feature is the lack of consensus as to the mechanisms that govern the emission of electrons. However, this feature is not surprising for a phenomenon that is critically dependent not only on the surface electronic properties of an as-yet poorly understood material but also on the

surface topography and the structural and compositional inhomogeneities that it exhibits.

5.2.2. Other Electronic Properties

Preliminary work has been carried out on the photoconductive behavior of RF magnetron–sputtered films [161, 162]. It has been found that the ratio between the dark and illuminated films was up to 5×10^6. Initial electroluminescence studies have also shown that amorphous carbon nitride films deposited onto aluminium-coated glass substrates luminesced with a blue–white emission for a short time under DC excitation with an electric field of approximately 4.6×10^5 V cm^{-1}.

There have been very few reports of any other "external" electronic properties other than field emission. One interesting recent paper reports the observation of a nonvolatile memory effect in carbon nitride films grown by FCA containing approximately 5% N [163]. These films were found to convert from a high-to a low-resistance state on the application of a reverse bias voltage. This observation was suggested to be due to an excitation of electrons from deep (acceptor) traps to shallower (donor) traps in which Poole–Frenkel conduction occurs by field-assisted thermionic emission of the electrons to the extended states in the conduction band rather than the hopping conduction that takes place between localized states at the Fermi level. The authors fabricated 1-bit memory cells with write times of 100 μs and memory retention of several months, suggesting that there may be a use for these films for digital information storage.

6. CONCLUSIONS

As can be gathered from the results described in the preceding text, the understanding of the electronic and optical properties of carbon nitride, whether the crystalline or the amorphous forms, is at a very rudimentary stage. For crystalline material, a number of predictions of band structure and density of states have been made but these are yet to be matched by any experimental evidence to confirm or contradict them. In noncrystalline material there is more experimental evidence but the variation in the composition and structure of the materials — whether it has high or low sp^3–sp^2 ratio, whether it contains high or low nitrogen levels, and whether it contains hydrogen or is hydrogen-free — means that drawing definite conclusions is extremely difficult. It is not at all clear how much the effects of incorporation of nitrogen depend on the nitrogen itself or on the consequent changes in carbon bonding that it causes. There are only a few basic conclusions that can be drawn with any degree of certainty:

1. Increasing the nitrogen content will, at relatively low levels, increase the sp^2 concentration, although it may increase again at high nitrogen contents.
2. Increasing the sp^2 content will increase the conductivity and reduce the optical gap.
3. Increasing the nitrogen content will introduce additional states into the valence band that act as donor levels producing n-type conductivity.

In terms of direct short-term utility in electronic devices, the main field of opportunity appears to be in the production of flat cathodes for field emission displays. It is clear, however, that the techniques for obtaining larger amounts of crystalline material are improving and it is likely that the resulting material, be it sp^3-bonded α- or β-C_3N_4 or sp^2-bonded quasi-fullerene will provide some major surprises, and the future electronic and optical uses of this interesting compound still remain to be discovered.

REFERENCES

1. N. N. Greenwood and A. Earnshaw, "The Chemistry of the Elements." Pergamon, New York, 1984.
2. S. A. Kajihara, A. Antonelli, R. Car, T. G. McAuley, D. M. Gruen, T. D. Corrigan, R. P. Chang, and H. Gnaser, *J. Appl. Phys.* 82, 4546 (1997).
3. D. I. Jones and A. D. Stewart, *Philos. Mag. B* 46, 432 (1982).
4. M. L. Cohen, *Phys. Rev. B* 32, 7988 (1985).
5. C. M. Sung, unpublished patent disclosure, (1984).
6. S. Matsumoto, E -Q. Xie, and F. Izumi, *Diamond Relat. Mater.* 8, 1175 (1999).
7. S. Vepřek, *Z. Phys. Chem.* 86, 95 (1973).
8. S. Vepřek, "Topics in Current Chemistry," Vol. 56, p. 140. Springer, Berlin, 1975.
9. J. J. Cuomo, P. A. Leary, D. Yu, W. Reuter, and M. Frisch, *J. Vac. Sci. Technol.* 16, 299 (1979).
10. A. Y. Liu and M. Cohen, *Phys. Rev. B* 41, 10727 (1990).
11. A. Y. Liu and M. Cohen, *Science* 245, 841 (1989).
12. C. M. Sung and M. Sung, *Mater. Chem. Phys.* 43, 1 (1996).
13. A. Y. Liu and R. M. Wentzcovitch, *Phys. Rev. B* 50, 10362 (1994).
14. J. C. Phillips, "Bonds and Bands in Semiconductors." Academic Press, New York, 1973.
15. C. Kittel, "Introduction to Solid State Physics," 6th ed. Wiley, New York, 1986.
16. F. D. Murnaghan, *Proc. Natl. Acad. Sci. U.S.A.* 30, 244 (1944).
17. Y. Guo and W. A. Goddard III, *Chem. Phys. Lett* 237, 72 (1995).
18. D. M. Teter and R. J. Hemley, *Science* 271, 53 (1996).
19. Y. Muramatsu, T. Hayashi, and R. C. C. Perera, *J. Electron. Spectrosc.* 104, 155 (1999).
20. Y. Miyamoto, M. L. Cohen, and S. G. Louie, *Solid State Commun.* 102, 605 (1997).
21. M. Coté, J. C. Grossman, M. L. Cohen, and S. G. Louie, *Phys. Rev. B* 58, 664 (1998).
22. H. Sjöstrom, W. Lanford, B. Hjörvarson, K. Xing, and J. -E. Sundgren, *J. Mater. Res.* 11, 981 (1996).
23. A. Kimura, T Ando, T Nishihara, and T Kato, U.S. Patent 4,664,976, 1987.
24. E. E. Haller, M. L. Cohen, and W. L. Hansen, U.S. Patent 5,110,679, 1992.
25. M. Matsumoto, Y Sato, M. Kamo, and N. Setaka, *Jpn. J. Appl. Phys.* 71, L183 (1982).

26. Y. Chen, L. Guo, and E. G. Wang, *Philos. Mag. Letts.* 75, 155 (1997).
27. A. Leonhardt, H Grügeŕ, D. Delbmann, B. Arnold, and J. Thomas, *Thin Solid Films* 332, 69 (1998).
28. S. F. Lim, T. S. Wee, J. Lin, D. H. C. Chua, and K. L. Tan, *J. Mater. Res.* 14, 1153 (1999).
29. R. Prioli, S. I. Zanette, A. O. Caride, D. F. Franceschini, and F. L. Freire, Jr., *J. Vac. Sci. Technol., A* 14, 2351 (1996).
30. H. Grüger, D. Selbmann, E. Wolf, A. Leonhardt, and B Arnold, *Surf. Coat. Technol.* 86–87, 409 (1996).
31. S. Miyake, Y. Setsuhara, K. Shibata, M. Kumagai, Y. Sakawa, T. Shoji, *Surf. Coat. Technol.* 116–119, 11 (1999).
32. K. Wu, E. G. Wang, J. Qing, and G. Xu, *J. Appl. Phys.* 83, 1702 (1998).
33. S. Bhattacharyya, C. Vallée, C. Cardinaud, O. Chauvet, and G. Turban, *J. Appl. Phys.* 85, 2162 (1999).
34. J. Kouvetakis and M. Todd, U.S. Patent 5,606,056 (1997).
35. S. Veprek, J. Weidmann, and F Glatz, *J. Vac. Sci. Technol., A* 13, 2914 (1995).
36. C. Popov, M. F. Plass, A. Bergmaier, and W. Kulisch, *Appl. Phys. A* 69, 241 (1999).
37. S. Matsumoto, K. K. Chattopadhyay, M. Mieno, and T. Ando, *J. Mater. Res.* 13, 180 (1998).
38. S. Muhl, A. Gaona-Couto, J. M. Méndez, S. Rodil, G. Gonzalez, A Merkulov, and R. Asomoza, *Thin Solid Films* 308–309, 228 (1997).
39. V. Hajek, K. Rusnak, J. Vlcek, L. Martinu, and S. J. Gujrathi, *J. Vac. Sci. Technol., A* 17, 899 (1999).
40. W. Kulisch, M. P. Delplancke-Ogletree, J. Bulir, M. Jelinek, J. Jurek, J. Zemek, and K. Klimovic, *Diamond Relat. Mater.* 8, 1039 (1999).
41. V. Hajek, K. Rusnak, J. Vlcek, L. Martinu, and S. C. Gujrathi, *J. Vac. Sci. Technol., A* 17, 899 (1999).
42. S. Lopez, M. -S. Wong, and W. D. Sproul, *J. Vac. Sci. Technol., A* 13, 1644 (1995).
43. Y. S. Jin, Y. Matsuda, and H. Fujiyama, *Jpn. J. Appl. Phys.* 37, 4544 (1998).
44. W. T. Zheng, E. Broitman, N. Hellgren, K. Z. Xing, H. Sjostrom, L. Hultman, and J. -E. Sundgren, *Thin Solid Films* 308–309, 223 (1997).
45. S. Kumar, K. S. A. Butcher, and T. L. Tansley, *J. Vac. Sci. Technol., A* 14, 2687 (1996).
46. N. Nakayama, Y. Tsuchiya, S. Tamada, K. Kosuge, S. Nagata, K. Takahiro, and S. Yamaguchi, *Jpn. J. Appl. Phys.* 32, L1465 (1993).
47. M. Gioti, S. Logothetidis, C. Charitidis, and H. Lefakis, *Vacuum* 53, 53 (1999).
48. A. K. M. S. Chowdhury, D. C. Cameron, M. S. J. Hashmi, and J. M. Gregg, *J. Mater. Sci.* 14, 2359 (1999).
49. M. A. Baker, P. Hammer, C. Lenardi, J. Haupt, and W Gissler, *Surf. Coat. Technol.* 97, 544 (1997).
50. S. Kobayashi, K. Miyazaki, S. Nozaki, H. Morisaki, S. Fukui, and S Masaki, *J. Vac. Sci. Technol., A* 14, 777 (1996).
51. C. Quiros, R. Nunez, P. Prieto, E. Elizalde, A. Fernandez, C. Schubert, C. Donnet, and J. M. Sanz, *Vacuum* 52, 199 (1999).
52. C. T. Kuo, L. C. Chen, K. H. Chen, T. M. Chen, and T. R. Lu, *Diamond Relat. Mater.* 8, 1724 (1999).
53. T. R. Lu, C. T. Kuo, J. R. Yang, L. C. Chen, K. H. Chen, and T. M. Chen, *Surf. Coat. Technol.* 115, 116 (1999).
54. Z. J. Zhang, S. Fan, J. Huang, and C. M. Lieber, *J. Electron. Mater.* 25, 57 (1996).
55. K. Yamamoto, Y. Koga, S. Fujiwara, F. Kokai, J. I. Kleiman, and K. K. Kim, *Thin Solid Films* 339, 38 (1999).
56. C. Niu, Y. Z. Lu, and C. M. Lieber, *Science* 261, 334 (1993).
57. M. Y. Chen and P. T. Murray, *J. Vac. Sci. Technol., A* 16, 2093 (1998).

58. I. Husein, Y. Z. Zhou, F. Li, R. C. Allen, C. Chan, J. I. Kleiman, Y. Gudimenko, and C. V. Cooper, *Mater. Sci. Eng., A* 209, 10 (1996).
59. J. Hartmann, P. Siemroth, B. Schultrich, and B Rauschenbach, *J. Vac. Sci. Technol., A* 15, 2983 (1997).
60. J. Koskinen, J. -P. Hirvonen, J. Levoska, and P. Torri, *Diamond Relat. Mater.* 5, 669 (1996).
61. Y. Taki, T. Kitagawa, and O. Takai, *Jpn. J. Appl. Phys.* 36, 4901 (1997).
62. C. Spaeth, M. Kuhn, T. Chudoba, and F. Richter, *Surf. Coat. Technol.* 112, 140 (1999).
63. S. R. P. Silva, J. Robertson, G. A. J. Amaratunga, B. Rafferty, L. M. Brown, J. Schwan, D. F. Franceschini, and G. Mariotto, *J. Appl. Phys.* 81, 2626 (1997).
64. P. H. Fang, U.S. Patent 5,405,515, 1993.
65. S. A. Korenev, A. J. Perry, A. Elkind, and A. Kalmukov, *Thin Solid Films* 308–309, 233 (1997).
66. F. Fujimoto and K. Ogata, *Jpn. J. Appl. Phys.* 32, L420 (1993).
67. M. Kohzaki, A. Matsumoro, T. Hayashi, M. Muramatsu, and K. Yamaguchi, *Thin Solid Films* 308–309, 239 (1997).
68. J. Q. Xie, Y. Zheng, and J. Y. Feng, *Nucl. Instrum. Methods* 122, 239 (1997).
69. A. Mansour and D. Ugolini, *Phys. Rev. B* 47, 10201 (1993).
70. K. J. Boyd, D. Marton, S. S. Todorov, A. H. Al-Bayati, J. Kulik, R. A. Zuhr, and J. W. Rabalais, *J. Vac. Sci. Technol.* 13, 2110 (1995).
71. N. Tsoubouchi, B. Enders, A. Chayahara, A. Kinomura, C. Heck, and Y. Horino, *J. Vac. Sci. Technol., A* 17, 2384 (1999).
72. S. Grigull, W. Jacob, D. Henke, C. Spaeth, L. Summchen, and W Sigle, *J. Appl. Phys.* 83, 5185 (1998).
73. P. -N. Wang, Z. Guo, X. -T. Ying, J-H. Chen, X. -M. Yu, and F. -M. Li, *Phys. Rev. B* 59, 13347 (1999).
74. I, Gouzman, R, Brener, and A, Hoffman, *J. Vac. Sci. Technol., A* 17, 411 (1999).
75. M. R. Wixom, *J. Am. Ceram. Soc.* 73, 1973 (1990).
76. J. H. Nguyen and R Jeanloz, *Mater. Sci. Eng., A* 209, 23 (1996).
77. Q. Fu, C. -B. Cao, and H. -S. Zhu, *J. Mater. Sci. Lett.* 18, 1485 (1999).
78. Q. Fu, J. -T. Jiu, K. Cai, H. Wang, C. -B. Cao, and H. -S. Zhu, *Phys. Rev. B* 59, 1693 (1999).
79. J. Widany, F. Weich, Th. Köhle, D. Porezag, and Th. Frauenheim, *Diamond Relat. Mater.* 5, 1031 (1996).
80. K. K. Mani and R. Ramini, *Phys. Stat. Solidi B* 61, 659 (1974).
81. R. J. Nemanich, G. Lucovsky, and S. A. Solin, *Solid State Commun.* 23, 117 (1977).
82. S. A. Solin, *Physica B* 99, 443 (1980).
83. R. J. Nemanich, G. Lucovsky, and S. A. Solin, in "Lattice Dynamics." (M. Balkanski, Ed.). Flammarion, Paris, 1975.
84. J. H. Kaufman, S. Metin, and D. D. Saperstein, *Phys. Rev. B* 39, 13053 (1989).
85. R. O. Dillon, J. A. Woolam, and V. Kathanant, *Phys. Rev. B* 29, 3482 (1994).
86. Y. Taki, T. Kitagawa, and O. Takai, *Thin Solid Films* 304, 183 (1997).
87. F. Tuinstra and J. L. Koenig, *J. Chem. Phys.* 53, 1126 (1970).
88. N. Hellgren, M. P. Johansson, E. Broitman, L. Hultman, and J. -E. Sundgren, *Phys. Rev. B* 59, 5162 (1999).
89. M. Schmitt, D. Paulmier, T. Le Huu, M. El Mansouri, A. Grabchenko, and A. G. Mamalis, *Thin Solid Films* 332, 124 (1998).
90. H. Raether, in "Springer Tracts in Modern Physics." (G. Höhler, Ed.), Vol. 88. Springer-Verlag, Berlin, 1980.
91. H. Cohen, E. Kolodnet, T. Maniv, and M. Folman, *Solid State Commun.* 81, 183 (1992).
92. H. Venghaus, *Phys. Status Solidi B* 71, 609 (1975).

93. F. R. McFeely, S. P. Kowalczyk, L. Ley, R. G. Cavell, R. A. Pollack, and D. A. Shirley, *Phys. Rev. B* 9, 5268 (1974).
94. J. M. Ripalda, E Román, N. Díaz, L. Galán, I. Montero, G. Comelli, A. Baraldi, S. Lizzit, A. Goldoni, and G. Paolucci, *Phys. Rev. B* 60, R3705 (1999).
95. J. L. He and W. L. Chang, *Surf. Coat. Technol.* 99, 184 (1998).
96. T. R. Lu, C. T. Kuo, J. R. Yang, L. C. Chen, K. H. Chen, and T. M. Chen, *Surf. Coat. Technol.* 115, 116 (1999).
97. D. X. Shi, X. F. Zhang, L. Yuan, Y. S. Gu, Y. P. Zhang, Z. J. Duan, X. R. Chang, Z. Z. Tian, and N. X. Chen, *Appl. Surf. Sci.* 148, 50 (1999).
98. A. K. M. S. Chowdhury, D. C. Cameron, and M. S. J. Hashmi, *Surf. Coat. Technol.* 112, 133 (1999).
99. A. K. M. S. Chowdhury, D. C. Cameron, and M. S. J. Hashmi, *Thin Solid Films* 332, 62 (1998).
100. N. B. Colthup, L. H. Daly, and S. E. Wiberly, "Introduction to Infrared and Raman Spectroscopy," 3rd ed. Academic Press, New York, 1990.
101. T. Werninghaus, D. S. R. T. Zahn, E. G. Wang, and Y. Chen, *Diamon Relat. Mater.* 7, 52 (1998).
102. D. Marton, K. J. Boyd, A. H. Al-Bayati, S. S. Todorov, and J. W. Rabalais, *Phys. Rev. Lett.* 73, 118 (1994).
103. C. Ronning, H. Feldermann, R. Merk, H. Hofsass, P. Reinke, and J. -U. Thiele, *Phys. Rev. B* 58, 2207 (1998).
104. P. Hammer, M. A. Baker, C. Lenardi, and W Gissler, *J. Vac. Sci. Technol., A* 15, 107 (1997).
105. J. Robertson, *Diamond Relat. Mater.* 2, 984 (1993).
106. V. S. Veeraswamy, J. Yuan, G. A. J. Amaratunga, W. I. Milne, K. W. R. Gilkes, M. Weiler, and L. M. Brown, *Phys. Rev. B* 48, 17954 (1993).
107. J. Hu, P. Yang, and C. M. Lieber, *Phys. Rev. B* 57, R3185 (1998).
108. N. Axen, G. A. Botton, H. Q. Lou, R. E. Somekh, and I. M. Hutchings, *Surf. Coat. Technol.* 81, 262 (1996).
109. M. A. Monclus, PhD thesis, Dublin City University (2000).
110. J. Stöhr, "NEXAFS Spectroscopy." Springer, Berlin, 1992.
111. Y. Duan, H. Zhang, and X. Xie, *Phys. Status Solidi B* 200, 499 (1997).
112. J. L. Corkill and M. L. Cohen, *Phys. Rev. B* 48, 17622 (1993).
113. X. Wang and P. J. Martin, *Appl. Phys. Lett.* 68, 1177 (1996).
114. J. Robertson and E. P. O'Reilly, *Phys. Rev. B* 35, 2946 (1987).
115. A. Ilie, N. M. J. Conway, B. Kleinsorge, J. Robertson, and W. I. Milne, *J. Appl. Phys.* 84, 5575 (1998).
116. V. S. Veeraswamy, G. A. J. Amaratunga, C. A. Davis, W. I. Milne, P. Hewitt, and M. Weiler, *Solid-State Electron.* 37, 319 (1994).
117. N. M. J. Conway, W. I. Milne, and J. Robertson, *Diamond Relat. Mater.* 7, 472 (1998).
118. J. Robertson and C. A. Davis, *Diamond Relat. Mater.* 4, 441 (1995).
119. D. Briggs and M. P.Seah, "Practical Surface Analysis by Auger and X-ray Photoelectron Spectroscopy." Wiley, New York, 1983.
120. S. Souto, S. Pickholz, M. C. dos Santos, and F. Alvarez, *Phys. Rev. B* 57, 2941 (1998).
121. M. C. dos Santos and F. Alvarez, *Phys. Rev. B* 58, 13918 (1998).
122. M. A. Monclus, D. C. Cameron, A. K. M. S. Chowdhury, R. Barklie, and M. Collins, *Surf. Coat. Technol.* 131, 488 (2000).
123. J. Tauc, in "Amorphous and Liquid Semiconductors." (J. Tauc, Ed.). Plenum, New York, 1974.
124. N. F. Mott and E. A. Davis, "Electronic Processes in Non-crystalline Solids," 2nd ed. Clarendon, Oxford, 1979.

125. S. John, C. Soukoulis, M. H. Cohen, and E. N. Economou, *Phys. Rev. Lett.* 57, 1777 (1986).
126. D. Dasgupta, C. De Martino, F. Demichelis, and A. Tagliaferro, *J. Non-Cryst. Solids* 164–166, 1147 (1993).
127. J. Robertson, *Philos. Mag. B* 66, 199 (1992).
128. M. Pelton, S. K. O'Leary, F. Gaspari, and S. Zukotynski, *J. Appl. Phys.* 83, 1029 (1998).
129. S. R. P. Silva, B. Rafferty, G. A. J. Amaratunga, J. Schwan, D. F. Franceschini, and L. M. Brown, *Diamond Relat. Mater.* 5, 401 (1996).
130. J. Schwan, V. Batori, S. Ulrich, H. Erhardt, and S. R. P. Silva, *J. Appl. Phys.* 84, 2071 (1998).
131. P. Hammer, N. M. Victoria, and F. Alvarez, *J. Vac. Sci. Technol., A* 16, 2941 (1998).
132. S. Lee, J. Park, S. Oh, W. M. Kim, J. H. Bae, B. Cheong, and S. G. Kim, *Thin Solid Films* 308–309, 135 (1997).
133. Y. F. Lu, Z. M. Ren, W. D. Song, and D. S. H. Chan, *J. Appl. Phys.* 84, 2133 (1998).
134. M. A. Monclus, D. C. Cameron, and A. K. M. S. Chowdhury, *Thin Solid Films* 341, 94 (1999).
135. J. Chen, A. X. Wei, S. Z. Deng, Y. Lu, G. Zheng, D. H. Chen, D. Mo, S. Q. Peng, and N. S. Xu, *J. Vac. Sci. Technol., B* 16, 697 (1998).
136. Z. Y. Chen, Y. H. Yu, J. P. Zhao, S. Q. Yang, T. S. Shi, X. H. Liu, E. Z. Luo, J. B. Xu, and I. H. Wilson, *Thin Solid Films* 339, 74 (1999).
137. N. Savvides, *J. Appl. Phys.* 59, 413 (1986).
138. F. W. Smith, *J. Appl. Phys.* 55, 764 (1984).
139. M. Chhowalla, I. Alexandrou, C. Kiely, G. A. J. Amaratunga, R. Aharonov, and R. F. Fontana, *Thin Solid Films* 290–291, 103 (1996).
140. T. Iwasaki, M. Aono, S. Nitta, H. Habuchi, T. Itoh, and S. Nonomura, *Diamond Relat. Mater.* 8, 440 (1999).
141. J. Szmidt, A. Jakubowski, and A. Balaninski, *Thin Solid films* 142, 269 (1986).
142. J. Szmidt, A. Werbowy, K. Sdunek, A. Sokowska, J. Konwerska-Hrabowska, and S. Mitura, *Diamond Relat. Mater.* 5, 564 (1996).
143. M. A. Baker, P. Hammer, C. Lenardi, J. Haupt, and W. Gissler, *Surf. Coat. Technol.* 97, 544 (1997).
144. Th. Frauenheim, U. Stephan, P. Blaudeck, and G. Jungnickel, *Diamond Relat. Mater.* 3, 462 (1994).
145. V. S. Veeraswamy, G. A. J. Amaratunga, W. I. Milne, P. Hewitt, P. J. Fallon, D. R. McKenzie, and C. A. Davis, *Diamond Relat. Mater.* 2, 782 (1993).
146. A. K. M. S. Chowdhury, D. C. Cameron, and M. A. Monclus, *Thin Solid Films* 355–356, 85 (1999).
147. C. A. Spindt, I Brodie, L. Humphrey, and E. R. Westerberg, *J. Appl. Phys.* 47, 5248 (1976).
148. K. Okano, S. Koizumi, S. R. Silva, and G. A. J. Amaratunga, *Nature* 398, 140 (1996).
149. T. Sugino, K. Kuriyama, C. Kimura, and S. Kawasaki, *Appl. Phys. Lett.* 73, 268 (1998).
150. K. Wu, E. G. Wang, J. Chen, and N. S. Xu, *J. Vac. Sci. Technol., B* 17, 1059 (1999).
151. B. S. Satyanarayana, A. Hart, W. I. Milne, and J. Robertson, *Appl. Phys. Lett.* 71, 1430 (1997).
152. N. Missert, T. A. Friedman, J. P. Sullivan, and R. G. Copeland, *Appl. Phys. Lett.* 70, 1995 (1997).
153. D. S. Mao, J. Zhao, W. Li, X. Ren, X. Wang, X. H. Liu, J. Y. Zhou, Z. Fan, Y. K. Zhu, Q. Li, and J. F. Xu, *J. Vac. Sci. Technol., B* 17, 311 (1999).
154. L. K. Cheah, X. Shi, and E. Liu, *Appl. Surf. Sci.* 143, 309 (1999).
155. E. J. Chi, J. Y. Shim, D. J. Choi, and H. K. Baik, *J. Vac. Sci. Technol., B* 16, 1219 (1998).
156. J. Chen, X. Wei, S. Z. Deng, Y. Lu, X. G. Zheng, D. H. Chen, D. Mo, S. Q. Peng, and N. S. Xu, *J. Vac. Sci. Technol., B* 16, 697 (1998).

157. N. Badi, A. Tempez, D. Starikov, A. Bensaoula, V. P. Ageev, A. Karabuov, M. V. Ugarov, V. Frolov, E. Loubnin, K. Waters, and A. Shultz, *J. Vac. Sci. Technol., A* 17, 1191 (1999).
158. M. Q. Ding, W. B. Choi, A. F. Myers, A. K. Sharma, J. Narayan, J. J. Cuomo, and J. J. Hren, *Surf. Coat. Technol.* 94–95, 672 (1997).
159. R. V. Latham, K. H. Bayliss, and B. M. Cox, *J. Phys. D: Appl. Phys.* 19, 214 (1980).
160. X. Shi, B. K. Tay, H. S. Tan, Z. Li, Y. Q. Tu, S. R. P. Silva, and W. I. Milne, *J. Appl. Phys.* 79, 7239 (1996).
161. N. Takada, K. Arai, and S. Nitta, *Appl. Surf. Sci.* 113, 274 (1997).
162. S. Nitta, N. Takada, K. Sugiyama, T. Itoh, and S. Nonomura, *J. Non-Cryst. Solids* 227–230, 655 (1998).
163. E. G. Gerstner and D. R. McKenzie, *J. Appl. Phys.* 84, 5647 (1998).